JOHANNES KEPLER UNIVERSITY LINZ

Institute of Computational Mathematics

Multiharmonic Finite Element Analysis of a Time-Periodic Parabolic Optimal Control Problem

Ulrich Langer
Institute of Computational Mathematics, Johannes Kepler University
Altenberger Str. 69, 4040 Linz, Austria

Monika Wolfmayr
Institute of Computational Mathematics, Johannes Kepler University
Altenberger Str. 69, 4040 Linz, Austria

NuMa-Report No. 2013-01 January 2013

A–4040 LINZ, Altenbergerstraße 69, Austria

Technical Reports before 1998:

1995

95-1	Hedwig Brandstetter *Was ist neu in Fortran 90?*	March 1995
95-2	G. Haase, B. Heise, M. Kuhn, U. Langer *Adaptive Domain Decomposition Methods for Finite and Boundary Element Equations.*	August 1995
95-3	Joachim Schöberl *An Automatic Mesh Generator Using Geometric Rules for Two and Three Space Dimensions.*	August 1995

1996

96-1	Ferdinand Kickinger *Automatic Mesh Generation for 3D Objects.*	February 1996
96-2	Mario Goppold, Gundolf Haase, Bodo Heise und Michael Kuhn *Preprocessing in BE/FE Domain Decomposition Methods.*	February 1996
96-3	Bodo Heise *A Mixed Variational Formulation for 3D Magnetostatics and its Finite Element Discretisation.*	February 1996
96-4	Bodo Heise und Michael Jung *Robust Parallel Newton-Multilevel Methods.*	February 1996
96-5	Ferdinand Kickinger *Algebraic Multigrid for Discrete Elliptic Second Order Problems.*	February 1996
96-6	Bodo Heise *A Mixed Variational Formulation for 3D Magnetostatics and its Finite Element Discretisation.*	May 1996
96-7	Michael Kuhn *Benchmarking for Boundary Element Methods.*	June 1996

1997

97-1	Bodo Heise, Michael Kuhn and Ulrich Langer *A Mixed Variational Formulation for 3D Magnetostatics in the Space $H(rot) \cap H(div)$*	February 1997
97-2	Joachim Schöberl *Robust Multigrid Preconditioning for Parameter Dependent Problems I: The Stokes-type Case.*	June 1997
97-3	Ferdinand Kickinger, Sergei V. Nepomnyaschikh, Ralf Pfau, Joachim Schöberl *Numerical Estimates of Inequalities in $H^{\frac{1}{2}}$.*	August 1997
97-4	Joachim Schöberl *Programmbeschreibung NAOMI 2D und Algebraic Multigrid.*	September 1997

From 1998 to 2008 technical reports were published by SFB013. Please see
`http://www.sfb013.uni-linz.ac.at/index.php?id=reports`
From 2004 on reports were also published by RICAM. Please see
`http://www.ricam.oeaw.ac.at/publications/list/`
For a complete list of NuMa reports see
`http://www.numa.uni-linz.ac.at/Publications/List/`

MULTIHARMONIC FINITE ELEMENT ANALYSIS OF A TIME-PERIODIC PARABOLIC OPTIMAL CONTROL PROBLEM

U. LANGER AND M. WOLFMAYR

Abstract. This paper presents the multiharmonic analysis of a distributed parabolic optimal control problem in a time-periodic setting. We prove the existence and uniqueness of the solution of some weak space-time variational formulation for the parabolic time-periodic boundary value problem appearing in the constraints for the optimal control problem. Since the cost functional is quadratic, the optimal control problem is uniquely solvable as well. In order to solve the optimal control problem, we state its optimality system and discretize it by the multiharmonic finite element method leading to a system of linear algebraic equations which decouples into smaller systems. We construct preconditioners for these systems which yield robust convergence rates and optimal complexity for the preconditioned minimal residual method. All systems can be solved totally in parallel. Furthermore, we present a complete analysis for the error introduced by the multiharmonic finite element discretization as well as some numerical results confirming our theoretical findings.

1. Introduction

This paper is devoted to distributed optimal control problems for parabolic time-periodic boundary value problems in bounded two- or three-dimensional Lipschitz domains. Such kind of problems can be found not only in electromagnetics but also in other technical applications, see, e.g., [1, 37]. Let us mention that in two space dimensions eddy current problems arising frequently in electromagnetics turn to parabolic problems. Time-periodic parabolic problems and their numerical solution were considered in [17, 38, 39, 28]. The unique solvability of parabolic initial-boundary value problems as well as of the parabolic problems in the time-periodic case is discussed in [42, 43]. In our work, we prove the unique solvability of a parabolic time-periodic boundary value problem in a special variational setting after introducing function spaces and formulating variational problems in the spirit of [27]. There are many papers on distributed optimal control problems for parabolic initial-boundary value problems, see, e.g., the recent paper [14] as well as the books [36, 9] and the references therein, but there are only a few papers on the time-periodic case, see [1, 19, 20] and [23, 22, 21]. The latter group of papers is devoted to the optimal control of time-periodic eddy current problems. In [1], the authors present a nested multigrid method for solving time-periodic parabolic optimal control problems. Our work considers the multiharmonic finite element method for solving these kind of problems, and we compare our numerical results to those obtained in [1]. The multiharmonic or the harmonic-balanced finite element method was successfully used for simulating electromagnetic devices which can be described by the eddy current approximation to Maxwell's equations, see [41, 31, 13, 16, 5, 6, 7, 12, 11]. Later the multiharmonic finite element method has been applied to time-periodic parabolic optimal control problems [19, 20, 26] and to time-periodic eddy current optimal control problems [23, 22, 21]. There are a couple of parameters involved in the time-periodic parabolic optimal control problem, e.g. the regularization or cost parameter as well as parameters which correspond to the conductivity and the reluctivity in practical applications in electromagnetics. Besides the discretization error analysis, the construction of fast solvers, which are

robust with respect to these "bad" parameters, are an important issue and a hot research topic during the last couple of years, see [18, 34, 44, 29, 32, 26].

In this paper, we provide a complete analysis of a time-periodic parabolic distributed optimal control problem and its multiharmonic finite element discretization. The discretization error analysis and the construction of robust solvers for the discrete optimality system are further contributions of this paper. More precisely, in Section 2, we state our time-periodic parabolic optimal control problem, investigate the unique solvability of the state equations in a special variational setting yielding the unique solvability of the optimal control problem. Finally, we derive the optimality system that we have to solve. Section 3 is devoted to the discretization of the optimality system by means of the multiharmonic finite element method. We expand the known desired state as well as the unknown state and co-state of the reduced optimality system into Fourier series and truncate them. The Fourier coefficients are then approximated by the finite element method. Due to the linearity and the orthogonality of the cosine and sine functions, the whole system of linear algebraic equations decouples into smaller systems depending only on the Fourier coefficients with respect to each single mode. Following [20], we construct preconditioners for our linear systems which yield robust convergence rates and optimal complexity for the preconditioned minimal residual (MINRES) method in Section 4. The preconditioners are practically implemented by a special algebraic multilevel iteration (AMLI) method that was proposed and analyzed in [24]. A complete analysis of the discretization error introduced by the multiharmonic finite element method is provided in Section 5. In Section 6, we present and discuss several numerical experiments to demonstrate the robustness and efficiency of the multiharmonic finite element method for solving time-periodic parabolic distributed optimal control problems. Finally, we draw some conclusions and give an outlook on some future work in Section 7.

2. A Time-Periodic Parabolic Optimal Control Problem

Let us denote the state of our optimal control problem by y and the control by u. The spatial domain $\Omega \subset \mathbb{R}^d$ is given by a bounded Lipschitz domain with the boundary $\Gamma := \partial\Omega$, where $d = 2, 3$. We mention that the numerical results presented in Section 6 were obtained for the case $d = 2$. Moreover, the space-time cylinder is denoted by $Q_T := \Omega \times (0,T)$ and its mantle boundary by $\Sigma_T := \Gamma \times (0,T)$. In this paper, we consider the following time-periodic parabolic distributed optimal control problem:

$$\min_{y,u} \mathcal{J}(y,u), \tag{1}$$

where the cost functional is given by the relation

$$\mathcal{J}(y,u) = \frac{1}{2}\int_0^T \int_\Omega [y(\boldsymbol{x},t) - y_d(\boldsymbol{x},t)]^2 \, d\boldsymbol{x}\, dt + \frac{\lambda}{2}\int_0^T \int_\Omega [u(\boldsymbol{x},t)]^2 \, d\boldsymbol{x}\, dt \tag{2}$$

subject to the time-periodic parabolic PDE (Partial Differential Equation) constraints

$$\begin{cases} \sigma(\boldsymbol{x})\dfrac{\partial}{\partial t} y(\boldsymbol{x},t) - \nabla\cdot(\nu(\boldsymbol{x})\nabla y(\boldsymbol{x},t)) = u(\boldsymbol{x},t), & (\boldsymbol{x},t) \in Q_T, \\ y(\boldsymbol{x},t) = 0, & (\boldsymbol{x},t) \in \Sigma_T, \\ y(\boldsymbol{x},0) = y(\boldsymbol{x},T), & \boldsymbol{x} \in \Omega, \end{cases} \tag{3}$$

with strictly positive and uniformly bounded coefficients σ and ν, i.e.

$$0 < \underline{\sigma} \le \sigma(\boldsymbol{x}) \le \overline{\sigma} \quad \text{and} \quad 0 < \underline{\nu} \le \nu(\boldsymbol{x}) \le \overline{\nu}, \quad \boldsymbol{x} \in \Omega.$$

The desired state y_d is the given target that we try to reach via a suitable control u. The positive regularization parameter λ provides a weighting of the cost of the control in the cost functional $\mathcal{J}(\cdot,\cdot)$.

In this section, we start with the existence and uniqueness proof for weak solutions of the PDE constraint described by (3), which guarantees the existence of a solution operator mapping the control space into the state space. This yields the existence of a unique solution of the optimal control problem (1)-(3). After that we formulate the optimality system of our problem.

2.1. **The PDE constraint.** First, we define proper function spaces which we will need for weak reformulations of our time-periodic problems, see, e.g., [27].

Definition 1. *The Sobolev space $H^{1,0}(Q_T)$ is defined by*

$$H^{1,0}(Q_T) = \{y \in L^2(Q_T) : \nabla y \in [L^2(Q_T)]^d\},$$

where ∇ is the weak spatial gradient, and equipped with the norm

$$\|y\|_{H^{1,0}(Q_T)} = \left(\int_0^T \int_\Omega \left(y(\boldsymbol{x},t)^2 + \left|\nabla y(\boldsymbol{x},t)\right|^2\right) d\boldsymbol{x}\, dt\right)^{1/2}.$$

The Sobolev space $H^{1,1}(Q_T)$ is defined by

$$H^{1,1}(Q_T) = \{y \in L^2(Q_T) : \nabla y \in [L^2(Q_T)]^d, \partial_t y \in L^2(Q_T)\},$$

where ∂_t denotes the weak time derivative, and equipped with the norm

$$\|y\|_{H^{1,1}(Q_T)} = \left(\int_0^T \int_\Omega \left(y(\boldsymbol{x},t)^2 + \left|\nabla y(\boldsymbol{x},t)\right|^2 + \left|\partial_t y(\boldsymbol{x},t)\right|^2\right) d\boldsymbol{x}\, dt\right)^{1/2}.$$

For $k = 0, 1$, the Sobolev space $H_0^{1,k}(Q_T)$ is defined by

$$H_0^{1,k}(Q_T) = \{y \in H^{1,k}(Q_T) : y = 0 \text{ on } \Sigma_T\},$$

whereas the Sobolev space $H_{0,per}^{1,1}(Q_T)$ is given by

$$H_{0,per}^{1,1}(Q_T) = \{y \in H_0^{1,1}(Q_T) : y(\boldsymbol{x},0) = y(\boldsymbol{x},T) \text{ for almost all } \boldsymbol{x} \in \Omega\}.$$

Moreover, the Sobolev spaces $H^{0,1}(Q_T)$ and $H_{per}^{0,1}(Q_T)$ are analogously defined as follows

$$H^{0,1}(Q_T) = \{y \in L^2(Q_T) : \partial_t y \in L^2(Q_T)\}$$

and

$$H_{per}^{0,1}(Q_T) = \{y \in H^{0,1}(Q_T) : y(\boldsymbol{x},0) = y(\boldsymbol{x},T) \text{ for almost all } \boldsymbol{x} \in \Omega\}.$$

For ease of notation, we will use the symbols $(\cdot,\cdot)_{L^2(\Omega)}$ and $\|\cdot\|_{L^2(\Omega)}$ as well as the symbols $(\cdot,\cdot)_{H^1(\Omega)}$ and $\|\cdot\|_{H^1(\Omega)}$ for indicating both the scalar and the vector-valued case. We denote the L^2-inner product by

$$(\boldsymbol{v},\boldsymbol{w})_{L^2(\Omega)} = \sum_{i=1}^n (v^i, w^i)_{L^2(\Omega)},$$

where $\boldsymbol{v} = (v^1, ..., v^n)^T$ and $\boldsymbol{w} = (w^1, ..., w^n)^T$ are vectors. The associated norm is given by

$$\|\boldsymbol{v}\|_{L^2(\Omega)}^2 = (\boldsymbol{v},\boldsymbol{v})_{L^2(\Omega)}.$$

In order to derive the space-time variational formulation, we multiply the parabolic PDE with a test function $v \in H_{0,per}^{1,1}(Q_T)$, integrate over the space-time cylinder Q_T, and after integration by parts, we obtain the following space-time variational

formulation of the PDE constraint: Given the right hand side $u \in L^2(Q_T)$, find $y \in H^{1,1}_{0,per}(Q_T)$ such that

$$\int_{Q_T} \left(\sigma(\boldsymbol{x}) \frac{\partial y}{\partial t} v + \nu(\boldsymbol{x}) \nabla y \cdot \nabla v \right) d\boldsymbol{x}\, dt = \int_{Q_T} u\, v\, d\boldsymbol{x}\, dt \quad \forall v \in H^{1,1}_{0,per}(Q_T). \tag{4}$$

Since all functions are at least from the space $L^2(Q_T)$, we can expand them into Fourier series. The Fourier series expansion in time, e.g., for y, is given by

$$y(\boldsymbol{x},t) = y_0^c(\boldsymbol{x}) + \sum_{k=1}^{\infty} \left(y_k^c(\boldsymbol{x}) \cos(k\omega t) + y_k^s(\boldsymbol{x}) \sin(k\omega t) \right) \tag{5}$$

with the Fourier coefficients

$$y_k^c(\boldsymbol{x}) = \frac{2}{T} \int_0^T y(\boldsymbol{x},t) \cos(k\omega t)\, dt \quad \text{and} \quad y_k^s(\boldsymbol{x}) = \frac{2}{T} \int_0^T y(\boldsymbol{x},t) \sin(k\omega t)\, dt, \tag{6}$$

where T and $\omega = 2\pi/T$ denote the periodicity and the frequency, respectively. In the following, we will use the notation

$$\boldsymbol{v}_k = (v_k^c, v_k^s)^T, \quad \boldsymbol{v}_k^\perp = (-v_k^s, v_k^c)^T \quad \text{and} \quad \nabla \boldsymbol{v}_k = ((\nabla v_k^c)^T, (\nabla v_k^s)^T)^T.$$

Inserting the Fourier series ansatz into the variational formulation (4), exploiting the orthogonality of the functions $\cos(k\omega t)$ and $\sin(k\omega t)$ with respect to the scalar product $(\cdot,\cdot)_{L^2(0,T)}$, we arrive at the following variational formulation corresponding to every single mode $k \in \mathbb{N}$: Given $\boldsymbol{u}_k \in (L^2(\Omega))^2$, find $\boldsymbol{y}_k \in \mathbb{V} := V \times V = (H_0^1(\Omega))^2$ such that

$$\int_\Omega \left(\nu(\boldsymbol{x}) \nabla \boldsymbol{y}_k(\boldsymbol{x}) \cdot \nabla \boldsymbol{v}_k(\boldsymbol{x}) + k\omega\sigma(\boldsymbol{x}) \boldsymbol{y}_k(\boldsymbol{x}) \cdot \boldsymbol{v}_k^\perp(\boldsymbol{x}) \right) d\boldsymbol{x} = \int_\Omega \boldsymbol{u}_k(\boldsymbol{x}) \cdot \boldsymbol{v}_k(\boldsymbol{x})\, d\boldsymbol{x} \tag{7}$$

for all $\boldsymbol{v}_k \in \mathbb{V}$. In the case $k = 0$, we obtain the following variational formulation: Given $u_0^c \in L^2(\Omega)$, find $y_0^c \in V = H_0^1(\Omega)$ such that

$$\int_\Omega \nu(\boldsymbol{x}) \nabla y_0^c(\boldsymbol{x}) \cdot \nabla v_0^c(\boldsymbol{x})\, d\boldsymbol{x} = \int_\Omega u_0^c(\boldsymbol{x}) v_0^c(\boldsymbol{x})\, d\boldsymbol{x}. \tag{8}$$

The space V is defined by

$$V = H_0^1(\Omega) = \{ y \in L^2(\Omega) : \nabla y \in L^2(\Omega) \text{ and } y = 0 \text{ on } \Gamma \}.$$

The space $\mathbb{V} = (H_0^1(\Omega))^2$ for the Fourier coefficients is equipped with the norm

$$\|\boldsymbol{y}_k\|^2_{H^1(\Omega)} = \|\boldsymbol{y}_k\|^2_{L^2(\Omega)} + \|\nabla \boldsymbol{y}_k\|^2_{L^2(\Omega)}.$$

Theorem 1. *The variational problems (7) and (8) have a unique solution.*

Proof. The proof follows from varifying the assumptions of the Lax-Milgram lemma and applying it. □

In order to prove existence and uniqueness of the space-time variational problem (4), we firstly prove the existence of a unique solution of a weaker variational formulation of our parabolic PDE (3). For that, we have to define additional special functions spaces.

Definition 2. *The function spaces $H^{0,\frac{1}{2}}(Q_T)$ and $H^{1,\frac{1}{2}}(Q_T)$ are defined by*

$$H^{0,\frac{1}{2}}(Q_T) = \{ y \in L^2(Q_T) : \left\| \partial_t^{1/2} y \right\|_{L^2(Q_T)} < \infty \}$$

and

$$H^{1,\frac{1}{2}}(Q_T) = \{ y \in H^{1,0}(Q_T) : \left\| \partial_t^{1/2} y \right\|_{L^2(Q_T)} < \infty \},$$

respectively, where $\left\| \partial_t^{1/2} y \right\|_{L^2(Q_T)}$ is defined in the Fourier space by the relation

$$\left\| \partial_t^{1/2} y \right\|^2_{L^2(Q_T)} := |y|^2_{H^{0,\frac{1}{2}}(Q_T)} := \frac{T}{2} \sum_{k=1}^{\infty} k\omega \|\boldsymbol{y}_k\|^2_{L^2(\Omega)}.$$

Hence, the corresponding inner product is analogously given by

$$\big(\partial_t^{1/2} y, \partial_t^{1/2} v\big)_{L^2(Q_T)} := \frac{T}{2} \sum_{k=1}^{\infty} k\omega (\boldsymbol{y}_k, \boldsymbol{v}_k)_{L^2(\Omega)},$$

and, in the same way, we define

$$\big(\partial_t^{1/2} y, \partial_t^{1/2} v^\perp\big)_{L^2(Q_T)} := \frac{T}{2} \sum_{k=1}^{\infty} k\omega (\boldsymbol{y}_k, \boldsymbol{v}_k^\perp)_{L^2(\Omega)}.$$

Moreover, we use the notation

$$\big(\sigma\partial_t^{1/2} y, \partial_t^{1/2} v\big)_{L^2(Q_T)} := \frac{T}{2} \sum_{k=1}^{\infty} k\omega (\sigma\boldsymbol{y}_k, \boldsymbol{v}_k)_{L^2(\Omega)} \quad \textit{and}$$

$$\big(\sigma\partial_t^{1/2} y, \partial_t^{1/2} v^\perp\big)_{L^2(Q_T)} := \frac{T}{2} \sum_{k=1}^{\infty} k\omega (\sigma\boldsymbol{y}_k, \boldsymbol{v}_k^\perp)_{L^2(\Omega)}$$

for the σ-weighted counterparts. The space $H_0^{1,\frac{1}{2}}(Q_T)$ is given by

$$H_0^{1,\frac{1}{2}}(Q_T) = \{y \in H^{1,\frac{1}{2}}(Q_T) : y = 0 \text{ on } \Sigma_T\}.$$

The seminorm and the norm of the space $H^{1,\frac{1}{2}}(Q_T)$ are defined in the Fourier space as follows:

$$|y|^2_{H^{1,\frac{1}{2}}} := T\|\nabla y_0^c\|^2_{L^2(\Omega)} + \frac{T}{2} \sum_{k=1}^{\infty} [k\omega \|\boldsymbol{y}_k\|^2_{L^2(\Omega)} + \|\nabla \boldsymbol{y}_k\|^2_{L^2(\Omega)}] \quad \textit{and}$$

$$\|y\|^2_{H^{1,\frac{1}{2}}} := T(\|y_0^c\|^2_{L^2(\Omega)} + \|\nabla y_0^c\|^2_{L^2(\Omega)}) + \frac{T}{2} \sum_{k=1}^{\infty} [(1+k\omega)\|\boldsymbol{y}_k\|^2_{L^2(\Omega)} + \|\nabla \boldsymbol{y}_k\|^2_{L^2(\Omega)}].$$

Furthermore, it is easy to see that the identities

$$\big(\partial_t^{1/2} y, \partial_t^{1/2} v\big)_{L^2(Q_T)} = \big(\partial_t y, v^\perp\big)_{L^2(Q_T)} \text{ and } \big(\partial_t^{1/2} y, \partial_t^{1/2} v^\perp\big)_{L^2(Q_T)} = \big(\partial_t y, v\big)_{L^2(Q_T)}$$

are valid for all $y \in H^{0,1}_{per}(Q_T)$ and $v \in H^{0,\frac{1}{2}}(Q_T)$. Indeed, inserting the Fourier expansions

$$\partial_t y(\boldsymbol{x}, t) := \sum_{k=1}^{\infty} [k\omega\, y_k^s(\boldsymbol{x}) \cos(k\omega t) - k\omega\, y_k^c(\boldsymbol{x}) \sin(k\omega t)] \text{ and}$$

$$v^\perp(\boldsymbol{x}, t) := \sum_{k=1}^{\infty} [y_k^s(\boldsymbol{x}) \cos(k\omega t) - y_k^c(\boldsymbol{x}) \sin(k\omega t)],$$

into the scalar products, we immediately get the identities given above. Furthermore, we obviously have $\|v\|_{L^2(Q_T)} = \|v^\perp\|_{L^2(Q_T)}$, and the orthogonality relations

$$\big(\partial_t y, y\big)_{L^2(Q_T)} = 0 \quad \text{and} \quad (y^\perp, y)_{L^2(Q_T)} = 0$$

for all $y \in H^{0,1}_{per}(Q_T)$, as well as

$$\big(\partial_t^{1/2} y, \partial_t^{1/2} y^\perp\big)_{L^2(Q_T)} = 0 \quad \text{and} \quad \big(\nabla y, \nabla y^\perp\big)_{L^2(Q_T)} = 0 \tag{9}$$

for all $y \in H^{1,\frac{1}{2}}(Q_T)$, which are also valid for their σ- and ν-weighted counterparts.

Now, we are in the position to state a more general variational formulation of our space-time variational problem (4): Given $u \in L^2(Q_T)$, find $y \in H_0^{1,\frac{1}{2}}(Q_T)$ such that

$$\int_{Q_T} \left(\sigma(\boldsymbol{x}) \frac{\partial^{1/2} y}{\partial t^{1/2}} \frac{\partial^{1/2} v^\perp}{\partial t^{1/2}} + \nu(\boldsymbol{x}) \nabla y \cdot \nabla v \right) d\boldsymbol{x}\, dt = \int_{Q_T} u\, v\, d\boldsymbol{x}\, dt \tag{10}$$

for all test functions $v \in H_0^{1,\frac{1}{2}}(Q_T)$, where all functions are given in their Fourier series expansion in time. More precisely, everything has to be understood in the sense of Definition 2. The following lemma provides the existence of a unique solution of variational problem (10) and serves as vehicle for the existence and uniqueness proof of the space-time variational problem (4) and, later, for the construction of preconditioners and the discretization error analysis.

Lemma 1. *The space-time bilinear form*

$$a(y,v) = \int_{Q_T} \left(\sigma(\boldsymbol{x}) \frac{\partial^{1/2} y}{\partial t^{1/2}} \frac{\partial^{1/2} v^\perp}{\partial t^{1/2}} + \nu(\boldsymbol{x}) \nabla y \cdot \nabla v \right) d\boldsymbol{x}\, dt$$

fulfills the following inf-sup and sup-sup conditions:

$$\mu_1 \|y\|_{H^{1,\frac{1}{2}}} \leq \sup_{0 \neq v \in H_0^{1,\frac{1}{2}}} \frac{a(y,v)}{\|v\|_{H^{1,\frac{1}{2}}}} \leq \mu_2 \|y\|_{H^{1,\frac{1}{2}}} \tag{11}$$

for all $y \in H_0^{1,\frac{1}{2}}$ *with positive constants* μ_1 *and* μ_2.

Proof. We start with the proof of the sup-sup condition. Using triangle and Cauchy-Schwarz' inequality, we obtain the estimate

$$\begin{aligned}
|a(y,v)| &= \Big| \int_{Q_T} \left(\sigma(\boldsymbol{x}) \frac{\partial^{1/2} y}{\partial t^{1/2}} \frac{\partial^{1/2} v^\perp}{\partial t^{1/2}} + \nu(\boldsymbol{x}) \nabla y \cdot \nabla v \right) d\boldsymbol{x}\, dt \Big| \\
&\leq \overline{\sigma} \Big| \int_{Q_T} \frac{\partial^{1/2} y}{\partial t^{1/2}} \frac{\partial^{1/2} v^\perp}{\partial t^{1/2}} \, d\boldsymbol{x}\, dt \Big| + \overline{\nu} \Big| \int_{Q_T} \nabla y \cdot \nabla v \, d\boldsymbol{x}\, dt \Big| \\
&\leq \overline{\sigma} \big\| \partial_t^{1/2} y \big\|_{L^2(Q_T)} \big\| \partial_t^{1/2} v \big\|_{L^2(Q_T)} + \overline{\nu} \|\nabla y\|_{L^2(Q_T)} \|\nabla v\|_{L^2(Q_T)} \\
&\leq \max\{\overline{\sigma}, \overline{\nu}\} |y|_{H^{1,\frac{1}{2}}} |v|_{H^{1,\frac{1}{2}}} \leq \mu_2 \|y\|_{H^{1,\frac{1}{2}}} \|v\|_{H^{1,\frac{1}{2}}}
\end{aligned}$$

with the constant $\mu_2 = \max\{\overline{\sigma}, \overline{\nu}\}$. Next, we prove the inf-sup condition by choosing the test function $v = y + y^\perp$. Using the σ- and ν-weighted orthogonality relations according to (9) and Friedrichs' inequality $\|y\|_{L^2(\Omega)} \leq c_F \|\nabla y\|_{L^2(\Omega)}$, we get

$$\begin{aligned}
a(y,y) &= \int_{Q_T} \left(\sigma(\boldsymbol{x}) \frac{\partial^{1/2} y}{\partial t^{1/2}} \frac{\partial^{1/2} y^\perp}{\partial t^{1/2}} + \nu(\boldsymbol{x}) \nabla y \cdot \nabla y \right) d\boldsymbol{x}\, dt = \int_{Q_T} \nu(\boldsymbol{x}) \nabla y \cdot \nabla y \, d\boldsymbol{x}\, dt \\
&\geq \underline{\nu} \int_{Q_T} |\nabla y|^2 \, d\boldsymbol{x}\, dt \geq \underline{\nu} \frac{1}{c_F^2 + 1} \|y\|^2_{H^{1,0}(Q_T)}
\end{aligned}$$

and

$$\begin{aligned}
a(y, y^\perp) &= \int_{Q_T} \left(\sigma(\boldsymbol{x}) \frac{\partial^{1/2} y}{\partial t^{1/2}} \frac{\partial^{1/2} y}{\partial t^{1/2}} + \nu(\boldsymbol{x}) \nabla y \cdot \nabla y^\perp \right) d\boldsymbol{x}\, dt \\
&= \int_{Q_T} \sigma(\boldsymbol{x}) \frac{\partial^{1/2} y}{\partial t^{1/2}} \frac{\partial^{1/2} y}{\partial t^{1/2}} \, d\boldsymbol{x}\, dt \geq \underline{\sigma} \big\| \partial_t^{1/2} y \big\|^2_{L^2(Q_T)}.
\end{aligned}$$

Altogether, we have

$$\begin{aligned}
a(y, y + y^\perp) &\geq \frac{\underline{\nu}}{c_F^2 + 1} \|y\|^2_{H^{1,0}(Q_T)} + \underline{\sigma} \big\| \partial_t^{1/2} y \big\|^2_{L^2(Q_T)} \\
&\geq \min\{ \frac{\underline{\nu}}{c_F^2 + 1}, \underline{\sigma} \} \left(\|y\|^2_{H^{1,0}(Q_T)} + \big\| \partial_t^{1/2} y \big\|^2_{L^2(Q_T)} \right) = \mu_1 \|y\|^2_{H^{1,\frac{1}{2}}(Q_T)}
\end{aligned}$$

with the constant $\mu_1 = \min\{ \frac{\underline{\nu}}{c_F^2+1}, \underline{\sigma} \}$. □

Theorem 2. *The space-time variational problem (10) has a unique solution.*

Proof. The proof follows immediately from Lemma 1 and from applying Babuška-Aziz' theorem which was established in [3] and [4]. □

Equipped with Lemma 1, we can prove existence and uniqueness of the following space-time variational problem which is weaker than the space-time variational problem (4) and also weaker than (10): Given $u \in L^2(Q_T)$, find $y \in H_0^{1,0}(Q_T)$ such that

$$\int_{Q_T} \left(-\sigma(\boldsymbol{x}) y \frac{\partial v}{\partial t} + \nu(\boldsymbol{x}) \nabla y \cdot \nabla v \right) d\boldsymbol{x}\, dt = \int_{Q_T} u\, v\, d\boldsymbol{x}\, dt \quad \forall v \in H_{0,per}^{1,1}(Q_T). \tag{12}$$

In order to prove existence and uniqueness of (12), we reuse some ideas known from the analysis of parabolic initial boundary value problems in [27], and adapt them to the time-periodic case.

Theorem 3. *The space-time variational problem (12) has a unique solution.*

Proof. We start with the uniqueness proof. Let us assume that there are two different solutions y_1 and $y_2 \in H_0^{1,0}(Q_T)$, $y_1 \neq y_2$, of the problem (12). We expand these two solutions into Fourier series in time, i.e.

$$y_1(\boldsymbol{x}, t) = \sum_{k=0}^{\infty} [y_{1k}^c(\boldsymbol{x}) \cos(k\omega t) + y_{1k}^s(\boldsymbol{x}) \sin(k\omega t)],$$

$$y_2(\boldsymbol{x}, t) = \sum_{k=0}^{\infty} [y_{2k}^c(\boldsymbol{x}) \cos(k\omega t) + y_{2k}^s(\boldsymbol{x}) \sin(k\omega t)],$$

whose unique Fourier coefficients are given by

$$y_{1k}^c(\boldsymbol{x}) = \frac{2}{T} \int_0^T y_1(\boldsymbol{x}, t) \cos(k\omega t)\, dt \quad \text{and} \quad y_{1k}^s(\boldsymbol{x}) = \frac{2}{T} \int_0^T y_1(\boldsymbol{x}, t) \sin(k\omega t)\, dt,$$

and

$$y_{2k}^c(\boldsymbol{x}) = \frac{2}{T} \int_0^T y_2(\boldsymbol{x}, t) \cos(k\omega t)\, dt \quad \text{and} \quad y_{2k}^s(\boldsymbol{x}) = \frac{2}{T} \int_0^T y_2(\boldsymbol{x}, t) \sin(k\omega t)\, dt.$$

Since $y_1 \neq y_2$, we have $y_{1k}^l(\boldsymbol{x}) \neq y_{2k}^l(\boldsymbol{x})$ for at least one $k \in \mathbb{N}_0$ and $l \in \{c, s\}$, and therefore $\boldsymbol{y_1}_k \neq \boldsymbol{y_2}_k$. Let us fix one arbitrary k for which $y_{1k}^l \neq y_{2k}^l$. For this k, we define

$$w_k^l := y_{2k}^l - y_{1k}^l \quad \text{and} \quad \boldsymbol{w}_k = (w_k^c, w_k^s)^T \in \mathbb{V} = V \times V = (H_0^1(\Omega))^2.$$

After inserting the Fourier series ansatz for y_1 and y_2 into the variational problem (12), the whole system decouples and we arrive at variational problems for the Fourier coefficients with respect to every single mode k, analogously as in (7) and (8). For the arbitrary but fixed k, we obtain the following variational problem: Find $\boldsymbol{w}_k \in \mathbb{V}$ such that

$$\underbrace{-\int_\Omega \sigma(\boldsymbol{x}) k\omega \boldsymbol{w}_k \cdot \boldsymbol{v}_k^\perp\, d\boldsymbol{x} + \int_\Omega \nu(\boldsymbol{x}) \nabla \boldsymbol{w}_k \cdot \nabla \boldsymbol{v}_k\, d\boldsymbol{x}}_{:= a_k(\boldsymbol{w}_k, \boldsymbol{v}_k)} = 0$$

for all $\boldsymbol{v}_k \in \mathbb{V}$. We choose the test function $\boldsymbol{v}_k = \boldsymbol{w}_k + \boldsymbol{w}_k^\perp$. Hence, we obtain

$$\begin{aligned} &-\int_\Omega \sigma(\boldsymbol{x}) k\omega (\boldsymbol{w}_k \cdot \boldsymbol{w}_k^\perp + \boldsymbol{w}_k \cdot (\boldsymbol{w}_k^\perp)^\perp)\, d\boldsymbol{x} \\ &\quad + \int_\Omega \nu(\boldsymbol{x}) (\nabla \boldsymbol{w}_k \cdot \nabla \boldsymbol{w}_k + \nabla \boldsymbol{w}_k \cdot \nabla \boldsymbol{w}_k^\perp)\, d\boldsymbol{x} = 0. \end{aligned}$$

From $(\boldsymbol{w}_k^\perp)^\perp = -\boldsymbol{w}_k$ and $\boldsymbol{w}_k \cdot \boldsymbol{w}_k^\perp = 0$ it follows that

$$\int_\Omega (\sigma(\boldsymbol{x}) k\omega \boldsymbol{w}_k \cdot \boldsymbol{w}_k + \nu(\boldsymbol{x}) \nabla \boldsymbol{w}_k \cdot \nabla \boldsymbol{w}_k)\, d\boldsymbol{x} = 0.$$

The bilinear form $a_k(\cdot,\cdot)$ is elliptic and bounded in the space $\mathbb{V} = V \times V = (H_0^1(\Omega))^2$. Hence, from

$$0 = a_k(\boldsymbol{w}_k, \boldsymbol{w}_k + \boldsymbol{w}_k^{\perp}) \geq \underline{\sigma} k\omega \int_\Omega \boldsymbol{w}_k \cdot \boldsymbol{w}_k \, d\boldsymbol{x} + \underline{\nu} \int_\Omega \nabla \boldsymbol{w}_k \cdot \nabla \boldsymbol{w}_k \, d\boldsymbol{x}$$
$$\geq \min\{\underline{\sigma} k\omega, \underline{\nu}\} \underbrace{\left(\int_\Omega \boldsymbol{w}_k \cdot \boldsymbol{w}_k + \nabla \boldsymbol{w}_k \cdot \nabla \boldsymbol{w}_k \, d\boldsymbol{x} \right)}_{= \|\boldsymbol{w}_k\|^2_{H^1(\Omega)}},$$

it follows that $\boldsymbol{w}_k = 0$ in $\mathbb{V}$. Since k was arbitrary, all Fourier coefficients of y_1 and y_2 have to be the same, hence $y_1 = y_2$, which is a contradiction to our assumption at the beginning. Thus, the uniqueness of a solution $y \in H_0^{1,0}(Q_T)$ of the variational problem (12) is proven. Now we come to the existence proof.

First, we want to prove that if $v \in H^{1,1}_{0,per}(Q_T)$ then the truncated Fourier series v_N converges weakly in $H^{1,1}_{0,per}(Q_T)$ to v. For that we expand v into a Fourier series in time, i.e.

$$v(\boldsymbol{x}, t) = \sum_{k=0}^{\infty} [v_k^c(\boldsymbol{x}) \cos(k\omega t) + v_k^s(\boldsymbol{x}) \sin(k\omega t)],$$

where the Fourier coefficients $v_k^l(\boldsymbol{x})$ with $l \in \{c, s\}$ are from $H_0^1(\Omega)$. Hence, the truncated Fourier series

$$v_N(\boldsymbol{x}, t) = \sum_{k=0}^{N} [v_k^c(\boldsymbol{x}) \cos(k\omega t) + v_k^s(\boldsymbol{x}) \sin(k\omega t)]$$

converges strongly in $L^2(Q_T)$ to v, i.e.

$$v_N \to v \quad \text{in } L^2(Q_T) \quad \text{for } N \to \infty.$$

It remains to show that

$$\nabla v_N \rightharpoonup \nabla v \quad \text{in } L^2(Q_T) \quad \text{for } N \to \infty$$

and

$$\frac{\partial v_N}{\partial t} \rightharpoonup \frac{\partial v}{\partial t} \quad \text{in } L^2(Q_T) \quad \text{for } N \to \infty.$$

Due to $v \in H^{1,1}_{0,per}(Q_T)$, the weak derivatives of v exist. Integration by parts and the periodicity of the test function $\varphi \in C^\infty_{per}(0,T)$ yield

$$\int_{Q_T} v_N(\boldsymbol{x}, t) \frac{\partial \varphi(t)}{\partial t} \, dt \, d\boldsymbol{x} = - \int_{Q_T} \frac{\partial v_N(\boldsymbol{x}, t)}{\partial t} \varphi(t) \, dt \, d\boldsymbol{x}$$

for all $\varphi \in C^\infty_{per}(0,T)$. We pass N to the limit and obtain

$$\int_{Q_T} v_N(\boldsymbol{x}, t) \frac{\partial \varphi(t)}{\partial t} \, dt \, d\boldsymbol{x} \longrightarrow \int_{Q_T} v(\boldsymbol{x}, t) \frac{\partial \varphi(t)}{\partial t} \, dt \, d\boldsymbol{x}.$$

So, there exists a $w \in L^2(Q_T)$ such that

$$\frac{\partial v_N(\boldsymbol{x}, t)}{\partial t} \rightharpoonup w \quad \text{in } L^2(Q_T) \quad \text{for } N \to \infty.$$

We define $\frac{\partial v}{\partial t} := w \in L^2(Q_T)$. Moreover, due to integration by parts it follows that

$$\int_{Q_T} \nabla v_N \cdot \boldsymbol{\varphi}(\boldsymbol{x}) \, d\boldsymbol{x} \, dt = - \int_{Q_T} v_N \, \nabla \cdot \boldsymbol{\varphi}(\boldsymbol{x}) \, d\boldsymbol{x} \, dt$$

for all $\boldsymbol{\varphi} \in [C_0^\infty(\Omega)]^d$, and $v_N \rightharpoonup v$ in $L^2(Q_T)$ yields

$$- \int_{Q_T} v_N \cdot \nabla \boldsymbol{\varphi}(\boldsymbol{x}) \, d\boldsymbol{x} \, dt \longrightarrow - \int_{Q_T} v \, \nabla \cdot \boldsymbol{\varphi}(\boldsymbol{x}) \, d\boldsymbol{x} \, dt.$$

Hence, there exists a $\boldsymbol{w} \in [L^2(Q_T)]^d$ such that

$$\nabla v_N \rightharpoonup \boldsymbol{w} \quad \text{in } [L^2(Q_T)]^d \quad \text{for } N \to \infty$$

and we define $\nabla v := \boldsymbol{w} \in [L^2(Q_T)]^d$. Altogether, it follows that $v_N \rightharpoonup v$ in $H^{1,1}_{0,per}(Q_T)$.

From Theorem 1 (especially from the orthogonalities of the cosine and sine functions) it follows that y_N solves the variational problem

$$\int_0^T \int_\Omega \left(-\sigma(\boldsymbol{x}) y_N \frac{\partial v_N}{\partial t} + \nu(\boldsymbol{x}) \nabla y_N \cdot \nabla v_N \right) d\boldsymbol{x}\, dt = \int_0^T \int_\Omega u\, v_N\, d\boldsymbol{x}\, dt,$$

where u is expanded into a Fourier series in time and y_N and v_N are truncated Fourier series in time. Moreover, y_N solves the variational problems (4) and (10) for all v_N, and $y_N, v_N \in H_0^{1,\frac{1}{2}}(Q_T)$. Choosing the test function $v_N = y_N + y_N^\perp$ and using Lemma 1, we get the estimates

$$\begin{aligned}
\|y_N\|^2_{H^{1,\frac{1}{2}}(Q_T)} &\leq \frac{1}{\mu_1} a(y_N, y_N + y_N^\perp) = \frac{1}{\mu_1} \int_0^T \int_\Omega u\, (y_N + y_N^\perp)\, d\boldsymbol{x}\, dt \\
&\leq \frac{1}{\mu_1} \|u\|_{L^2(Q_T)} \|y_N + y_N^\perp\|_{L^2(Q_T)} \\
&\leq \frac{1}{\mu_1} \|u\|_{L^2(Q_T)} 2 \|y_N\|_{L^2(Q_T)} \\
&\leq \frac{2}{\mu_1} \|u\|_{L^2(Q_T)} \|y_N\|_{H^{1,\frac{1}{2}}(Q_T)}.
\end{aligned}$$

Hence, y_N is bounded, i.e.

$$\|y_N\|_{H^{1,\frac{1}{2}}(Q_T)} \leq \frac{2}{\mu_1} \|u\|_{L^2(Q_T)} < \infty. \tag{13}$$

Moreover,

$$\|y_N\|_{L^2(Q_T)} \leq \|y_N\|_{H^{1,0}(Q_T)} \leq \|y_N\|_{H^{1,\frac{1}{2}}(Q_T)}. \tag{14}$$

From estimate (13) it follows that

$$y_N \rightharpoonup y \quad \text{in } H_0^{1,\frac{1}{2}}(Q_T) \quad \text{for } N \to \infty,$$

hence

$$y_N \rightharpoonup y \quad \text{in } H_0^{1,0}(Q_T) \quad \text{for } N \to \infty.$$

It remains to show that y solves our variational problem (12).

Let us choose $M \in \mathbb{N}$ arbitrarily and $N \in \mathbb{N}$ with $N \leq M$, where $v_M \rightharpoonup v$ in $H^{1,1}_{0,per}(Q_T)$ and $u_N \to u$ in $L^2(Q_T)$. Inserting y_N, u_N and the arbitrary test function v_M into the variational problem (12) yields

$$\int_0^T \int_\Omega \left(-\sigma(\boldsymbol{x}) y_N \frac{\partial v_M}{\partial t} + \nu(\boldsymbol{x}) \nabla y_N \cdot \nabla v_M \right) d\boldsymbol{x}\, dt = \int_0^T \int_\Omega u_N\, v_M\, d\boldsymbol{x}\, dt.$$

Since the test function $v_M \rightharpoonup v$ in $H^{1,1}_{0,per}(Q_T)$ for $M \to \infty$,

$$\int_0^T \int_\Omega \left(-\sigma(\boldsymbol{x}) y_N \frac{\partial v}{\partial t} + \nu(\boldsymbol{x}) \nabla y_N \cdot \nabla v \right) d\boldsymbol{x}\, dt = \int_0^T \int_\Omega u_N\, v\, d\boldsymbol{x}\, dt.$$

Now we pass N to the limit. Since $u_N \to u$ in $L^2(Q_T)$ and $y_N \rightharpoonup y$ in $H_0^{1,0}(Q_T)$, we finally get

$$\int_0^T \int_\Omega \left(-\sigma(\boldsymbol{x}) y \frac{\partial v}{\partial t} + \nu(\boldsymbol{x}) \nabla y \cdot \nabla v \right) d\boldsymbol{x}\, dt = \int_0^T \int_\Omega u\, v\, d\boldsymbol{x}\, dt,$$

which means that $y \in H_0^{1,0}(Q_T)$ solves the variational problem (12). □

Remark 1. *Together with (13) it follows the existence and uniqueness of a solution of the variational problem (12) in the space* $H_0^{1,\frac{1}{2}}(Q_T)$ *as well. The variational problems (10) and (12) are equivalent.*

Remark 2. *If we assume that* $\nabla \cdot (\nu \nabla y) \in L^2(Q_T)$*, then* $y \in H^{1,1}_{0,per}(Q_T)$*. Hence, we obtain immediately existence and uniqueness of the variational problem (4) and we derive naturally the periodicity condition for* y *in a weak sense. More precisely, from* $\nabla \cdot (\nu \nabla y) \in L^2(Q_T)$ *and integration by parts of (12) it follows that*

$$\int_{Q_T} -\sigma(\boldsymbol{x}) y \, \frac{\partial v}{\partial t} \, d\boldsymbol{x} \, dt = \int_{Q_T} \nabla \cdot (\nu(\boldsymbol{x}) \nabla y) \, v \, d\boldsymbol{x} \, dt + \int_{Q_T} u \, v \, d\boldsymbol{x} \, dt$$

for all test functions $v \in H^{1,1}_{0,per}(Q_T)$*. Hence, the weak time derivative of* y *is defined, i.e.*

$$\int_{Q_T} -\sigma(\boldsymbol{x}) y \, \frac{\partial v}{\partial t} \, d\boldsymbol{x} \, dt = \int_{Q_T} \underbrace{(\nabla \cdot (\nu(\boldsymbol{x}) \nabla y) + u)}_{=: \sigma(\boldsymbol{x}) \frac{\partial y}{\partial t}} v \, d\boldsymbol{x} \, dt$$

with $\sigma \frac{\partial y}{\partial t} \in L^2(Q_T)$*. So the problem (12) together with* $\nabla \cdot (\nu \nabla y) \in L^2(Q_T)$ *is equivalent to*

$$\int_{Q_T} \sigma(\boldsymbol{x}) \frac{\partial y}{\partial t} \, v \, d\boldsymbol{x} \, dt - \int_\Omega \sigma(\boldsymbol{x}) \left(y(\boldsymbol{x}, T) v(\boldsymbol{x}, T) - y(\boldsymbol{x}, 0) v(\boldsymbol{x}, 0) \right) d\boldsymbol{x} + \int_{Q_T} \nabla \cdot (\nu(\boldsymbol{x}) \nabla y) \, v \, d\boldsymbol{x} \, dt = \int_{Q_T} u \, v \, d\boldsymbol{x} \, dt$$

for all $v \in H^{1,1}_{0,per}(Q_T)$*. Since* v *is periodic,*

$$\int_{Q_T} \sigma(\boldsymbol{x}) \frac{\partial y}{\partial t} \, v \, d\boldsymbol{x} \, dt - \int_\Omega \sigma(\boldsymbol{x}) (y(\boldsymbol{x}, T) - y(\boldsymbol{x}, 0)) v(\boldsymbol{x}, 0) \, d\boldsymbol{x} + \int_{Q_T} \nabla \cdot (\nu(\boldsymbol{x}) \nabla y) \, v \, d\boldsymbol{x} \, dt = \int_{Q_T} u \, v \, d\boldsymbol{x} \, dt$$

and

$$\int_{Q_T} \left(\sigma(\boldsymbol{x}) \frac{\partial y}{\partial t} - \nabla \cdot (\nu(\boldsymbol{x}) \nabla y) - u \right) v \, d\boldsymbol{x} \, dt = \int_\Omega \sigma(\boldsymbol{x}) (y(\boldsymbol{x}, T) - y(\boldsymbol{x}, 0)) v(\boldsymbol{x}, 0) \, d\boldsymbol{x}$$

for all $v \in H^{1,1}_{0,per}(Q_T)$*. Choose* $v \in H^{1,1}_{0,per}(Q_T)$ *such that* $v(\boldsymbol{x}, 0) = 0$ *for almost all* $\boldsymbol{x} \in \Omega$*. Hence,*

$$\int_{Q_T} \left(\sigma(\boldsymbol{x}) \frac{\partial y}{\partial t} - \nabla \cdot (\nu(\boldsymbol{x}) \nabla y) - u \right) v \, d\boldsymbol{x} \, dt = 0$$

for all $v \in H^{1,1}_{0,per}(Q_T)$ *and so*

$$\sigma(\boldsymbol{x}) \frac{\partial y}{\partial t} - \nabla \cdot (\nu(\boldsymbol{x}) \nabla y) - u = 0$$

in $L^2(Q_T)$*. It follows that*

$$\int_\Omega \sigma(\boldsymbol{x}) (y(\boldsymbol{x}, T) - y(\boldsymbol{x}, 0)) v(\boldsymbol{x}, 0) \, d\boldsymbol{x} = 0$$

for all $v \in H^{1,1}_{0,per}(Q_T)$ *and this yields*

$$y(\boldsymbol{x}, T) - y(\boldsymbol{x}, 0) = 0$$

for almost all $\boldsymbol{x} \in \Omega$*.*

Remark 3. *Under classical regularity assumptions imposed on* y*, e.g.,* $y \in C^2(\overline{Q}_T)$*, and on the data* u, σ, ν*, e.g.,* $u \in C(\overline{Q}_T)$*,* $\sigma \in C(\overline{\Omega})$*,* $\nu \in C^1(\overline{\Omega})$*, it follows that* y *is the unique solution of the state equation (3).*

Theorem 2 implies the existence of a linear and continuous solution operator which uniquely assigns a state $y \in H_0^{1,\frac{1}{2}}(Q_T)$ to every control $u \in L^2(Q_T)$, where the space $H_0^{1,\frac{1}{2}}(Q_T)$ is compactly embedded in $L^2(Q_T)$. With the solution operator, the optimal control problem (1)-(3) can be rewritten as a reduced minimization problem. The existence of its unique solution can be analogously proven as, e.g., in [36] under the assumptions that $y_d \in L^2(Q_T)$ and $\lambda > 0$. Note that here (3) has to be understood in a weak sense, more precisely, in the sense of (10).

2.2. **The optimality system.** We want to formulate now the optimality system. Its solution is equivalent to the solution of the original optimal control problem (1)-(3). Let us denote the Lagrange multiplier by p. We choose the following Lagrange functional for our minimization problem:

$$\mathcal{L}(y,u,p) := \mathcal{J}(y,u) - \int_0^T \int_\Omega \Big(\sigma \frac{\partial y}{\partial t} - \nabla \cdot \big(\nu \nabla y\big) - u\Big) p \, d\boldsymbol{x}\, dt. \tag{15}$$

The three conditions

$$\begin{cases} \nabla_y \mathcal{L}(y,u,p) = 0, \\ \nabla_u \mathcal{L}(y,u,p) = 0, \\ \nabla_p \mathcal{L}(y,u,p) = 0, \end{cases} \tag{16}$$

are called optimality system and characterize a stationary point (y,u,p) of the Lagrange functional (15). Using the second condition, we eliminate the control u from the optimality system (16), i.e.

$$u = -\lambda^{-1} p \ \text{ in } \ Q_T. \tag{17}$$

Note that the Lagrange multiplier p is also refered as the co-state. From (17) it appears very natural to choose y, p and also u all from the same space, see [20]. Moreover, we arrive at a reduced optimality system, written in its classical formulation as

$$\begin{cases} \sigma(\boldsymbol{x}) \dfrac{\partial}{\partial t} y(\boldsymbol{x},t) - \nabla \cdot (\nu(\boldsymbol{x}) \nabla y(\boldsymbol{x},t)) = -\lambda^{-1} p(\boldsymbol{x},t), & (\boldsymbol{x},t) \in Q_T, \\ y(\boldsymbol{x},t) = 0, & (\boldsymbol{x},t) \in \Sigma_T, \\ y(\boldsymbol{x},0) = y(\boldsymbol{x},T), & \boldsymbol{x} \in \Omega, \\ -\sigma(\boldsymbol{x}) \dfrac{\partial}{\partial t} p(\boldsymbol{x},t) - \nabla \cdot (\nu(\boldsymbol{x}) \nabla p(\boldsymbol{x},t)) = y(\boldsymbol{x},t) - y_d(\boldsymbol{x},t), & (\boldsymbol{x},t) \in Q_T, \\ p(\boldsymbol{x},t) = 0, & (\boldsymbol{x},t) \in \Sigma_T, \\ p(\boldsymbol{x},T) = p(\boldsymbol{x},0), & \boldsymbol{x} \in \Omega. \end{cases} \tag{18}$$

The space-time variational formulation of (18) is obtained in the same way as for the PDE constraint (10) in Subsection 2.1 and is stated as the following: Given the desired state $y_d \in L^2(Q_T)$, find y and p from $H_0^{1,\frac{1}{2}}(Q_T)$ such that

$$\begin{cases} \displaystyle\int_{Q_T} \Big(y\, v - \nu(\boldsymbol{x}) \nabla p \cdot \nabla v + \sigma(\boldsymbol{x}) \frac{\partial^{1/2} p}{\partial t^{1/2}} \frac{\partial^{1/2} v^\perp}{\partial t^{1/2}} \Big)\, d\boldsymbol{x}\, dt = \int_{Q_T} y_d\, v \, d\boldsymbol{x}\, dt, \\ \displaystyle\int_{Q_T} \Big(\nu(\boldsymbol{x}) \nabla y \cdot \nabla q + \sigma(\boldsymbol{x}) \frac{\partial^{1/2} y}{\partial t^{1/2}} \frac{\partial^{1/2} q^\perp}{\partial t^{1/2}} + \lambda^{-1} p\, q \Big)\, d\boldsymbol{x}\, dt = 0 \end{cases} \tag{19}$$

for all test functions $v, q \in H_0^{1,\frac{1}{2}}(Q_T)$, where all functions are given in their Fourier series expansion in time according to Definition 2.

3. Multiharmonic Finite Element Discretization

In order to solve our optimal control problem (1)-(3), we solve the optimality system (19) by a multiharmonic finite element discretization. We approximate the desired state y_d by truncating its Fourier series expansion and arrive at

$$y_d(\boldsymbol{x},t) \approx \sum_{k=0}^{N} [y_{dk}^c(\boldsymbol{x})\cos(k\omega t) + y_{dk}^s(\boldsymbol{x})\sin(k\omega t)] = y_{dN}(\boldsymbol{x},t), \tag{20}$$

where its Fourier coefficients are given by

$$y_{dk}^c(\boldsymbol{x}) = \frac{2}{T}\int_0^T y_d(\boldsymbol{x},t)\cos(k\omega t)\,dt \;\text{ and }\; y_{dk}^s(\boldsymbol{x}) = \frac{2}{T}\int_0^T y_d(\boldsymbol{x},t)\sin(k\omega t)\,dt. \tag{21}$$

We mention here that in general we have to compute the Fourier coefficients numerically, but for the moment we consider only the case where we can compute the Fourier coefficients exactly. In the case that y_d has really a multiharmonic representation, we refer to [20].

We insert the truncated desired state and the Fourier series ansatz of the state y and the co-state p into the space-time variational formulation (19). From the orthogonality of the functions $\cos(k\omega t)$ and $\sin(k\omega t)$ it follows that it is sufficient to consider only the truncated Fourier series of y and p, i.e.

$$\begin{cases} y(\boldsymbol{x},t) \approx \sum_{k=0}^{N} [y_k^c(\boldsymbol{x})\cos(k\omega t) + y_k^s(\boldsymbol{x})\sin(k\omega t)] = y_N(\boldsymbol{x},t), \\ p(\boldsymbol{x},t) \approx \sum_{k=0}^{N} [p_k^c(\boldsymbol{x})\cos(k\omega t) + p_k^s(\boldsymbol{x})\sin(k\omega t)] = p_N(\boldsymbol{x},t). \end{cases} \tag{22}$$

We arrive at the following system which has to be solved for every mode $k = 1,2,...,N$: Find $\boldsymbol{y}_k, \boldsymbol{p}_k \in \mathbb{V} = V \times V = (H_0^1(\Omega))^2$ such that

$$\begin{cases} \int_\Omega \left(\boldsymbol{y}_k \cdot \boldsymbol{v}_k - \nu(\boldsymbol{x})\nabla \boldsymbol{p}_k \cdot \nabla \boldsymbol{v}_k + k\omega\sigma(\boldsymbol{x})\boldsymbol{p}_k \cdot \boldsymbol{v}_k^\perp\right) d\boldsymbol{x} = \int_\Omega \boldsymbol{y_{d}}_k \cdot \boldsymbol{v}_k \, d\boldsymbol{x}, \\ \int_\Omega \left(\nu(\boldsymbol{x})\nabla \boldsymbol{y}_k \cdot \nabla \boldsymbol{q}_k + k\omega\sigma(\boldsymbol{x})\boldsymbol{y}_k \cdot \boldsymbol{q}_k^\perp + \lambda^{-1}\boldsymbol{p}_k \cdot \boldsymbol{q}_k\right) d\boldsymbol{x} = 0 \end{cases} \tag{23}$$

for all test functions $\boldsymbol{v}_k, \boldsymbol{q}_k \in \mathbb{V} = V \times V$.

In the case of $k = 0$, we obtain the following optimality system: Find $y_0^c, p_0^c \in V = H_0^1(\Omega)$ such that

$$\begin{cases} \int_\Omega \left(y_0^c \cdot v_0^c - \nu(\boldsymbol{x})\nabla p_0^c \cdot \nabla v_0^c\right) d\boldsymbol{x} = \int_\Omega y_{d0}^c \cdot v_0^c \, d\boldsymbol{x}, \quad \forall v_0^c \in V = H_0^1(\Omega) \\ \int_\Omega \left(\nu(\boldsymbol{x})\nabla y_0^c \cdot \nabla q_0^c + \lambda^{-1} p_0^c \cdot q_0^c\right) d\boldsymbol{x} = 0, \quad \forall q_0^c \in V = H_0^1(\Omega). \end{cases} \tag{24}$$

We want to approximate the unknown Fourier coefficients $\boldsymbol{y}_k = (y_k^c, y_k^s)^T$, $\boldsymbol{p}_k = (p_k^c, p_k^s)^T \in \mathbb{V}$ by finite element functions $\boldsymbol{y}_{kh} = (y_{kh}^c, y_{kh}^s)^T$, $\boldsymbol{p}_{kh} = (p_{kh}^c, p_{kh}^s)^T \in \mathbb{V}_h = V_h \times V_h \subset \mathbb{V}$. The space $\mathbb{V}_h = V_h \times V_h$ is a finite element space, where $V_h = \text{span}\{\varphi_1, ..., \varphi_n\}$ with the standard nodal basis $\{\varphi_i(x) = \varphi_{ih}(x) : i = 1,2,...,n_h\}$ and h denotes the usual discretization parameter such that $n = n_h = \dim V_h = O(h^{-d})$. We will use continuous, piecewise linear finite elements on triangles (2d) and tetrahedrons (3d) on a regular triangulation to construct the finite element subspace V_h and its basis in our numerical experiments, see [10]. This yields the

following linear system arising from the variational formulation (23):

$$\begin{pmatrix} M_h & 0 & -K_h & k\omega M_{h,\sigma} \\ 0 & M_h & -k\omega M_{h,\sigma} & -K_h \\ -K_h & -k\omega M_{h,\sigma} & -\lambda^{-1}M_h & 0 \\ k\omega M_{h,\sigma} & -K_h & 0 & -\lambda^{-1}M_h \end{pmatrix} \begin{pmatrix} \underline{y}_k^c \\ \underline{y}_k^s \\ \underline{p}_k^c \\ \underline{p}_k^s \end{pmatrix} = \begin{pmatrix} \underline{y}_{dk}^c \\ \underline{y}_{dk}^s \\ 0 \\ 0 \end{pmatrix}, \tag{25}$$

which has to be solved with respect to the nodal parameter vectors $\underline{y}_k^j = \underline{y}_{kh}^j = (y_{k,i}^j)_{i=1,\dots,n} \in \mathbb{R}^n$ and $\underline{p}_k^j = \underline{p}_{kh}^j = (p_{k,i}^j)_{i=1,\dots,n} \in \mathbb{R}^n$ of the finite element approximations

$$y_{kh}^j(x) = \sum_{i=1}^n y_{k,i}^j \varphi_i(x) \quad \text{and} \quad p_{kh}^j(x) = \sum_{i=1}^n p_{k,i}^j \varphi_i(x) \tag{26}$$

to the unknown Fourier coefficients $y_k^j(x)$ and $p_k^j(x)$ with $j \in \{c, s\}$. The matrix M_h, $M_{h,\sigma}$ and K_h correspond to the mass matrix, the weighted mass matrix and the weighted stiffness matrix, respectively. Their entries are computed by the following formulas:

$$M_h^{ij} = \int_\Omega \varphi_i \varphi_j \, d\boldsymbol{x}, \qquad M_{h,\sigma}^{ij} = \int_\Omega \sigma \varphi_i \varphi_j \, d\boldsymbol{x}, \qquad K_h^{ij} = \int_\Omega \nu \nabla \varphi_i \cdot \nabla \varphi_j \, d\boldsymbol{x},$$

with $i, j = 1, ..., n$, whereas

$$\underline{y}_{dk}^c = \Big[\int_\Omega y_{dk}^c \varphi_j \, d\boldsymbol{x} \Big]_{j=1,\dots,n} \quad \text{and} \quad \underline{y}_{dk}^s = \Big[\int_\Omega y_{dk}^s \varphi_j \, d\boldsymbol{x} \Big]_{j=1,\dots,n}.$$

In the case $k = 0$, we obtain the following linear system arising from the variational problem (24):

$$\begin{pmatrix} M_h & -K_h \\ -K_h & -\lambda^{-1}M_h \end{pmatrix} \begin{pmatrix} \underline{y}_0^c \\ \underline{p}_0^c \end{pmatrix} = \begin{pmatrix} \underline{y}_{d0}^c \\ 0 \end{pmatrix}. \tag{27}$$

From the solutions of the linear systems (25) and (27) we can easily reconstruct the multiharmonic finite element approximations of the state $y(\boldsymbol{x}, t)$ and the co-state $p(\boldsymbol{x}, t)$, i.e.

$$\begin{cases} y_{Nh}(\boldsymbol{x}, t) = \sum_{k=0}^N [y_{kh}^c(\boldsymbol{x}) \cos(k\omega t) + y_{kh}^s(\boldsymbol{x}) \sin(k\omega t)], \\ p_{Nh}(\boldsymbol{x}, t) = \sum_{k=0}^N [p_{kh}^c(\boldsymbol{x}) \cos(k\omega t) + p_{kh}^s(\boldsymbol{x}) \sin(k\omega t)]. \end{cases} \tag{28}$$

We will present an error analyis for the complete discretization error between the unknown solution (y, p) and its multiharmonic finite element approximation (y_{Nh}, p_{Nh}) in Section 5.

4. The inf-sup and sup-sup Condition and Robust Preconditioning

The linear system (25) as well as the system (27) are saddle point problems of the form

$$\underbrace{\begin{pmatrix} A & B^T \\ B & -C \end{pmatrix}}_{=:\mathcal{A}} \begin{pmatrix} \underline{y} \\ \underline{p} \end{pmatrix} = \underbrace{\begin{pmatrix} \underline{f} \\ 0 \end{pmatrix}}_{=:f}. \tag{29}$$

In the case $k = 1, ..., N$, we have that

$$A := \begin{pmatrix} M_h & 0 \\ 0 & M_h \end{pmatrix}, \; B := \begin{pmatrix} -K_h & -k\omega M_{h,\sigma} \\ k\omega M_{h,\sigma} & -K_h \end{pmatrix}, \; C := \lambda^{-1} A$$

and

$$\underline{f} := \begin{pmatrix} \underline{y}^c_{dk} \\ \underline{y}^s_{dk} \end{pmatrix}, \ \underline{y} := \begin{pmatrix} \underline{y}^c_k \\ \underline{y}^s_k \end{pmatrix}, \ \underline{p} := \begin{pmatrix} \underline{p}^c_k \\ \underline{p}^s_k \end{pmatrix}.$$

Saddle point problems of the form (29) can be solved by a preconditioned MINRES method, see [30]. Hence, it is crucial to construct preconditioners, which yield robust and fast convergence for the preconditioned MINRES method. In Subsection 4.1 and 4.2, we follow [20] by constructing such preconditioners.

4.1. **Robust Preconditioning.** In [20], the authors constructed preconditioners for the case that the parameter σ is constant, hence $M_{h,\sigma} = \sigma M_h$, by following the strategy presented in [44]. The idea is to construct two preconditioners which yield robust convergence rates for the preconditioned MINRES method and apply the operator interpolation theorem, which is based on the construction of intermediate spaces via the so called real interpolation method. The ideas of the real method (J- and the K-method) are due to Lions and Peetre and the theory of the real method is developed e.g. in [8], see also [2]. Finally, in [20], the authors arrive at the following preconditioner for the system (29) in the case where σ is constant:

$$\mathcal{P} = \begin{pmatrix} D & 0 & 0 & 0 \\ 0 & D & 0 & 0 \\ 0 & 0 & \lambda^{-1}D & 0 \\ 0 & 0 & 0 & \lambda^{-1}D \end{pmatrix} \tag{30}$$

with the block diagonal matrices $D := \sqrt{\lambda}K_h + (k\omega\sigma\sqrt{\lambda} + 1)M_h$. This yields the following condition number estimate:

$$\kappa_{\mathcal{P}}(\mathcal{P}^{-1}\mathcal{A}) \leq \overline{c}/\underline{c}$$

with constants $\overline{c}$, $\underline{c}$ independent of all involved parameters.

In the case that the parameter σ is only piecewise constant, hence $M_{h,\sigma} \neq \sigma M_h$ and

$$\mathcal{A} := \begin{pmatrix} M_h & 0 & -K_h & k\omega M_{h,\sigma} \\ 0 & M_h & -k\omega M_{h,\sigma} & -K_h \\ -K_h & -k\omega M_{h,\sigma} & -\lambda^{-1}M_h & 0 \\ k\omega M_{h,\sigma} & -K_h & 0 & -\lambda^{-1}M_h \end{pmatrix}, \tag{31}$$

we cannot apply the operator interpolation theory anymore. According to [20], we take the block diagonal preconditioner $\mathcal{P}$ and replace σM_h by $M_{h,\sigma}$ in (30). Hence, we arrive at the new preconditioner $\mathcal{P}$ but with $D := \sqrt{\lambda}K_h + k\omega\sqrt{\lambda}M_{h,\sigma} + M_h$. The goal is to obtain robust norm estimates for the preconditioned system matrix $\mathcal{P}^{-1}\mathcal{A}$. In [20], the authors were able to verify the assumptions of Babuška-Aziz' theorem, which are equivalent to the norm estimates for the precondioned system matrix. In the following, we will summarize their results. We define the following bilinear form arising from the optimality system (23):

$$\begin{aligned} \mathcal{B}((\boldsymbol{y}_k, \boldsymbol{p}_k), (\boldsymbol{v}_k, \boldsymbol{q}_k)) := &\int_\Omega \boldsymbol{y}_k \cdot \boldsymbol{v}_k - \nu\nabla\boldsymbol{p}_k \cdot \nabla\boldsymbol{v}_k + k\omega\sigma\boldsymbol{p}_k \cdot \boldsymbol{v}_k^\perp \, d\boldsymbol{x} \\ &+ \int_\Omega \nu\nabla\boldsymbol{y}_k \cdot \nabla\boldsymbol{q}_k + k\omega\sigma\boldsymbol{y}_k \cdot \boldsymbol{q}_k^\perp + \lambda^{-1}\boldsymbol{p}_k \cdot \boldsymbol{q}_k \, d\boldsymbol{x}. \end{aligned} \tag{32}$$

Hence, the variational problem (23) now reads as follows: Find $(\boldsymbol{y}_k, \boldsymbol{p}_k) \in \mathbb{V}^2 = \mathbb{V} \times \mathbb{V} = (H_0^1(\Omega))^4$ such that

$$\mathcal{B}((\boldsymbol{y}_k, \boldsymbol{p}_k), (\boldsymbol{v}_k, \boldsymbol{q}_k)) = \int_\Omega \boldsymbol{y_d}_k \cdot \boldsymbol{v}_k \, d\boldsymbol{x} \tag{33}$$

for all test functions $(\boldsymbol{v}_k, \boldsymbol{q}_k) \in \mathbb{V}^2$.

We define the following inner products and associated norms inspired by the preconditioner $\mathcal{P}$, which we need in order to prove the assumptions of Babuška-Aziz' theorem. We first define an inner product in $\mathbb{V} = (H_0^1(\Omega))^2$ by

$$(\boldsymbol{y}_k, \boldsymbol{v}_k)_{\mathbb{V}} = \sqrt{\lambda}\,(\nu\nabla\boldsymbol{y}_k, \nabla\boldsymbol{v}_k)_{L^2(\Omega)} + k\omega\sqrt{\lambda}\,(\sigma\boldsymbol{y}_k, \boldsymbol{v}_k)_{L^2(\Omega)} + (\boldsymbol{y}_k, \boldsymbol{v}_k)_{L^2(\Omega)} \tag{34}$$

with the associated norm

$$\|\boldsymbol{y}_k\|_{\mathbb{V}}^2 = \sqrt{\lambda}\,(\nu\nabla\boldsymbol{y}_k, \nabla\boldsymbol{y}_k)_{L^2(\Omega)} + k\omega\sqrt{\lambda}\,(\sigma\boldsymbol{y}_k, \boldsymbol{y}_k)_{L^2(\Omega)} + \|\boldsymbol{y}_k\|_{L^2(\Omega)}^2, \tag{35}$$

which differs from the standard H^1-norms. Next, we define an inner product in $\mathbb{V}^2 = (H_0^1(\Omega))^4$ by

$$((\boldsymbol{y}_k, \boldsymbol{p}_k), (\boldsymbol{v}_k, \boldsymbol{q}_k))_{\mathcal{P}} = (\boldsymbol{y}_k, \boldsymbol{v}_k)_{\mathbb{V}} + \lambda^{-1}(\boldsymbol{p}_k, \boldsymbol{q}_k)_{\mathbb{V}} \tag{36}$$

with the associated norm

$$\|(\boldsymbol{y}_k, \boldsymbol{p}_k)\|_{\mathcal{P}}^2 = \|\boldsymbol{y}_k\|_{\mathbb{V}}^2 + \lambda^{-1}\|\boldsymbol{p}_k\|_{\mathbb{V}}^2. \tag{37}$$

The following theorem verifies the assumptions of Babuška-Aziz' theorem, which are equivalent to the norm estimates for our preconditioned system $\mathcal{P}^{-1}\mathcal{A}$. Moreover, it follows the existence and uniqueness of the solution of the variational problem (33) due to the theorem of Babuška-Aziz.

Theorem 4. *The following inequalities*

$$\underline{c}\,\|(\boldsymbol{y}_k, \boldsymbol{p}_k)\|_{\mathcal{P}} \leq \sup_{0\neq(\boldsymbol{v}_k,\boldsymbol{q}_k)\in\mathbb{V}^2} \frac{\mathcal{B}((\boldsymbol{y}_k, \boldsymbol{p}_k), (\boldsymbol{v}_k, \boldsymbol{q}_k))}{\|(\boldsymbol{v}_k, \boldsymbol{q}_k)\|_{\mathcal{P}}} \leq \overline{c}\,\|(\boldsymbol{y}_k, \boldsymbol{p}_k)\|_{\mathcal{P}} \tag{38}$$

hold for all $(\boldsymbol{y}_k, \boldsymbol{p}_k) \in \mathbb{V}^2$ *with constants* $\underline{c} = 1/\sqrt{3}$ *and* $\overline{c} = 1$.

Proof. See [20]. □

In the discrete case, we can repeat the proof of Theorem 4 step-by-step replacing $\mathbb{V}^2$ by $\mathbb{V}_h^2$, and we finally arrive at the same inequalities with the same constants. In matrix-vector notation, we have proven the inequalities

$$\underline{c}\,\|\underline{x}\|_{\mathcal{P}} \leq \sup_{\underline{z}\in\mathbb{R}^{4n}} \frac{(\mathcal{A}\underline{x}, \underline{z})}{\|\underline{z}\|_{\mathcal{P}}} \leq \overline{c}\,\|\underline{x}\|_{\mathcal{P}} \quad \forall \underline{x} \in \mathbb{R}^{4n} \tag{39}$$

implying the condition number estimate

$$\kappa_{\mathcal{P}}(\mathcal{P}^{-1}\mathcal{A}) := \|\mathcal{P}^{-1}\mathcal{A}\|_{\mathcal{P}}\,\|\mathcal{A}^{-1}\mathcal{P}\|_{\mathcal{P}} \leq \overline{c}/\underline{c} = \sqrt{3}, \tag{40}$$

which yields the following robust convergence rate of the preconditioned MINRES method:

$$q = \frac{\kappa_{\mathcal{P}}(\mathcal{P}^{-1}\mathcal{A}) - 1}{\kappa_{\mathcal{P}}(\mathcal{P}^{-1}\mathcal{A}) + 1} \leq \frac{\sqrt{3} - 1}{\sqrt{3} + 1} \approx 0.267949,$$

see [20] and the references therein, e.g., [15].

The preconditioner for the discretized system (27) in the case of $k = 0$ is analogously determined (cf. [20]). It follows the preconditioner

$$P = \begin{pmatrix} D & 0 \\ 0 & \lambda^{-1}D \end{pmatrix} \tag{41}$$

with the diagonal block matrix $D := M_h + \sqrt{\lambda}K_h$. In this case, we obtain the following condition number estimate:

$$\kappa_{\mathcal{P}}(\mathcal{P}^{-1}\mathcal{A}) \leq \sqrt{2}, \tag{42}$$

which provides a robust convergence rate of the preconditioned MINRES method with

$$q \leq \frac{\sqrt{2} - 1}{\sqrt{2} + 1} \approx 0.171573,$$

see [20]. In a nutshell, we have designed preconditioners for the linear systems (25) and (27) corresponding to the modes $1 \le k \le N$ and $k = 0$, respectively, providing robust convergence rates for solving the preconditioned system by the preconditioned MINRES method.

4.2. **Practical Implementation.** In practical applications, for a large number of degrees of freedom, it is not very efficient to invert the preconditioners $\mathcal{P}$ in (30) of the discretized problem (25) for the case $0 < k \le N$ and P in (41) of the problem (27) for the case $k = 0$ exactly. Hence, it is important to replace the diagonal blocks $D = \sqrt{\lambda}K_h + k\omega\sqrt{\lambda}M_{h,\sigma} + M_h$ of the preconditioner $\mathcal{P}$ and the diagonal blocks $D = M_h + \sqrt{\lambda}K_h$ of the preconditioner P by diagonal blocks $\tilde{D}$, which are spectrally equivalent to D, robust, symmetric positive definite and more cost efficient. Such practical preconditioners $\tilde{\mathcal{P}}$ can be obtained by various methods like DD (domain decomposition), AMG (algebraic multigrid) or AMLI (algebraic multilevel iteration) methods, see, e.g., [35, 25, 40, 33]. Hence, we get a new practical preconditioner, e.g., for the case $0 < k \le N$, i.e.

$$\tilde{\mathcal{P}} = \begin{pmatrix} \tilde{D} & 0 & 0 & 0 \\ 0 & \tilde{D} & 0 & 0 \\ 0 & 0 & \lambda^{-1}\tilde{D} & 0 \\ 0 & 0 & 0 & \lambda^{-1}\tilde{D} \end{pmatrix} \tag{43}$$

with $\underline{c}_D\tilde{D} \le D \le \overline{c}_D\tilde{D}$ leading to the following robust condition number estimate:

$$\kappa_{\tilde{\mathcal{P}}}(\tilde{\mathcal{P}}^{-1}\mathcal{A}) \le \kappa_{\mathcal{P}}(\mathcal{P}^{-1}\mathcal{A})\,(\overline{c}_D/\underline{c}_D), \tag{44}$$

where $\kappa_{\mathcal{P}}(\mathcal{P}^{-1}\mathcal{A})$ can be estimated by (40) for $0 < k \le N$ and by (42) for $k = 0$. In Section 6, we will present some numerical results using an AMLI preconditioner proposed in [24].

5. Discretization Error Analysis

For the complete error analysis, we have to define norms in certain function spaces inspired by the $\mathcal{P}$-norm and similar to the definitions (34)-(37).

Definition 3. *We define the following function spaces:*

$$V_0 := H_0^{1,\frac{1}{2}}(Q_T),$$
$$V_1 := (H^{0,\frac{1}{2}})_0^1(Q_T) \cap H_{per}^{0,1}(Q_T),$$

where

$$(H^{0,\frac{1}{2}})_0^1(Q_T) := \{v \in H^{0,\frac{1}{2}}(Q_T) : \nabla v \in H^{0,\frac{1}{2}}(Q_T),\, v = 0 \ on\ \Sigma_T\}$$

with corresponding norms

$$\|y\|_{V_0}^2 = \|y\|_{L^2(Q_T)}^2 + \sqrt{\lambda}\,(\nu\nabla y, \nabla y)_{L^2(Q_T)} + \sqrt{\lambda}\big(\sigma\partial_t^{1/2}y, \partial_t^{1/2}y\big)_{L^2(Q_T)},$$
$$\begin{aligned}\|y\|_{V_1}^2 &= \|y\|_{L^2(Q_T)}^2 + \big\|\partial_t^{1/2}y\big\|_{L^2(\Omega)}^2 + \sqrt{\lambda}\,(\nu\nabla y, \nabla y)_{L^2(Q_T)} \\ &\quad + \sqrt{\lambda}\big(\nu\partial_t^{1/2}\nabla y, \partial_t^{1/2}\nabla y\big)_{L^2(Q_T)} + \sqrt{\lambda}\big(\sigma\partial_t y, \partial_t y\big)_{L^2(Q_T)},\end{aligned}$$

all defined in the Fourier space according to Definition 2, i.e.

$$\begin{aligned}
\|y\|_{V_0}^2 &= T(\|y_0^c\|_{L^2(\Omega)}^2 + \sqrt{\lambda}(\nu\nabla y_0^c, \nabla y_0^c)_{L^2(\Omega)}) \\
&\quad + \frac{T}{2}\sum_{k=1}^{\infty}[\|\boldsymbol{y}_k\|_{L^2(\Omega)}^2 + \sqrt{\lambda}(\nu\nabla\boldsymbol{y}_k, \nabla\boldsymbol{y}_k)_{L^2(\Omega)} + \sqrt{\lambda}k\omega(\sigma\boldsymbol{y}_k, \boldsymbol{y}_k)_{L^2(\Omega)}], \\
\|y\|_{V_1}^2 &= T(\|y_0^c\|_{L^2(\Omega)}^2 + \sqrt{\lambda}(\nu\nabla y_0^c, \nabla y_0^c)_{L^2(\Omega)}) \\
&\quad + \frac{T}{2}\sum_{k=1}^{\infty}[(1+k\omega)\|\boldsymbol{y}_k\|_{L^2(\Omega)}^2 + \sqrt{\lambda}(1+k\omega)(\nu\nabla\boldsymbol{y}_k, \nabla\boldsymbol{y}_k)_{L^2(\Omega)} \\
&\quad + \sqrt{\lambda}(k\omega)^2(\sigma\boldsymbol{y}_k, \boldsymbol{y}_k)_{L^2(\Omega)}].
\end{aligned}$$

Moreover, we define the following vector-valued norms as well:

$$\begin{aligned}
\|(y,p)\|_{P_0}^2 &= \|y\|_{V_0}^2 + \lambda^{-1}\|p\|_{V_0}^2 \\
\|(y,p)\|_{P_1}^2 &= \|y\|_{V_1}^2 + \lambda^{-1}\|p\|_{V_1}^2.
\end{aligned}$$

Remark 4. *Note that the $\mathbb{V}$-norm defined in (35) as well as the $\mathcal{P}$-norm defined in (37) correspond to the V_0-norm and the P_0-norm, respectively, for a single mode k, i.e.*

$$\begin{aligned}
\|y\|_{V_0}^2 &= T\|y_0^c\|_V^2 + \frac{T}{2}\sum_{k=1}^{\infty}\|\boldsymbol{y}_k\|_{\mathbb{V}}^2 \\
\|(y,p)\|_{P_0}^2 &= T\|(y_0^c, p_0^c)\|_P^2 + \frac{T}{2}\sum_{k=1}^{\infty}\|(\boldsymbol{y}_k, \boldsymbol{p}_k)\|_{\mathcal{P}}^2.
\end{aligned}$$

The complete discretization error between the exact solution of the variational problem (19) and its multiharmonic finite element approximation is given by

$$\|(y,p) - (y_{Nh}, p_{Nh})\|_{P_0}, \tag{45}$$

where the exact solution is expanded into Fourier series, i.e.

$$\begin{aligned}
y(\boldsymbol{x},t) &= y_0^c(\boldsymbol{x}) + \sum_{k=1}^{\infty}[y_k^c(\boldsymbol{x})\cos(k\omega t) + y_k^s(\boldsymbol{x})\sin(k\omega t)], \\
p(\boldsymbol{x},t) &= p_0^c(\boldsymbol{x}) + \sum_{k=1}^{\infty}[p_k^c(\boldsymbol{x})\cos(k\omega t) + p_k^s(\boldsymbol{x})\sin(k\omega t)],
\end{aligned}$$

and their multiharmonic finite element approximations are given by

$$\begin{aligned}
y_{Nh}(\boldsymbol{x},t) &= y_{0h}^c(\boldsymbol{x}) + \sum_{k=1}^{N}[y_{kh}^c(\boldsymbol{x})\cos(k\omega t) + y_{kh}^s(\boldsymbol{x})\sin(k\omega t)], \\
p_{Nh}(\boldsymbol{x},t) &= p_{0h}^c(\boldsymbol{x}) + \sum_{k=1}^{N}[p_{kh}^c(\boldsymbol{x})\cos(k\omega t) + p_{kh}^s(\boldsymbol{x})\sin(k\omega t)].
\end{aligned}$$

Using triangle inequality, we can split the discretization error (45) into two parts, i.e.

$$\|(y,p) - (y_{Nh}, p_{Nh})\|_{P_0} \leq \underbrace{\|(y,p) - (y_N, p_N)\|_{P_0}}_{\text{discretization error in } N} + \underbrace{\|(y_N, p_N) - (y_{Nh}, p_{Nh})\|_{P_0}}_{\text{discretization error in } h}.$$

5.1. **Discretization error in N.** The following theorem provides an estimate for the discretization error due to truncation of the Fourier series at the mode N.

Theorem 5. *Let us assume that $y, p \in V_1$. Then the discretization error due to truncation of the Fourier series can be estimated by*

$$\|(y,p) - (y_N, p_N)\|_{P_0} \leq c_0 \frac{1}{\sqrt{N}} \|(y,p)\|_{P_1}, \tag{46}$$

where c_0 is a constant depending only on the frequency ω.

Proof. The P_0-norm is given by

$$\|(y,p) - (y_N, p_N)\|^2_{P_0} = \|y - y_N\|^2_{V_0} + \lambda^{-1} \|p - p_N\|^2_{V_0}.$$

Under the assumption that $y \in V_1 = (H^{0,\frac{1}{2}})^1_0(Q_T) \cap H^{0,1}_{per}(Q_T)$, we obtain the following estimate:

$$\begin{aligned}
\|y - y_N\|^2_{V_0} &= \frac{T}{2} \sum_{k=N+1}^{\infty} \Big[\|\boldsymbol{y}_k\|^2_{L^2(\Omega)} + \sqrt{\lambda}(\nu \nabla \boldsymbol{y}_k, \nabla \boldsymbol{y}_k)_{L^2(\Omega)} + \sqrt{\lambda} k\omega (\sigma \boldsymbol{y}_k, \boldsymbol{y}_k)_{L^2(\Omega)} \Big] \\
&\leq \frac{T}{2} \sum_{k=N+1}^{\infty} \left[\frac{1+k\omega}{k\omega} \|\boldsymbol{y}_k\|^2_{L^2(\Omega)} + \sqrt{\lambda} \frac{1+k\omega}{k\omega} (\nu \nabla \boldsymbol{y}_k, \nabla \boldsymbol{y}_k)_{L^2(\Omega)} \right. \\
&\qquad \left. + \sqrt{\lambda} \frac{(k\omega)^2}{k\omega} (\sigma \boldsymbol{y}_k, \boldsymbol{y}_k)_{L^2(\Omega)} \right] \\
&\leq \frac{T}{2} \max_{k \geq N+1} \frac{1}{k\omega} \sum_{k=N+1}^{\infty} \Big[(1+k\omega) \|\boldsymbol{y}_k\|^2_{L^2(\Omega)} \\
&\qquad + \sqrt{\lambda}(1+k\omega)(\nu \nabla \boldsymbol{y}_k, \nabla \boldsymbol{y}_k)_{L^2(\Omega)} + \sqrt{\lambda}(k\omega)^2 (\sigma \boldsymbol{y}_k, \boldsymbol{y}_k)_{L^2(\Omega)} \Big] \\
&\leq \frac{1}{(N+1)\omega} \frac{T}{2} \sum_{k=N+1}^{\infty} \Big[(1+k\omega) \|\boldsymbol{y}_k\|^2_{L^2(\Omega)} \\
&\qquad + \sqrt{\lambda}(1+k\omega)(\nu \nabla \boldsymbol{y}_k, \nabla \boldsymbol{y}_k)_{L^2(\Omega)} + \sqrt{\lambda}(k\omega)^2 (\sigma \boldsymbol{y}_k, \boldsymbol{y}_k)_{L^2(\Omega)} \Big] \\
&\leq c_0^2 \frac{1}{N} \|y\|^2_{V_1},
\end{aligned}$$

where $c_0 = c_0(\omega) = 1/\sqrt{\omega}$. Altogether we obtain for $y, p \in V_1$ the following estimate:

$$\begin{aligned}
\|(y,p) - (y_N, p_N)\|^2_{P_0} &= \|y - y_N\|^2_{V_0} + \lambda^{-1} \|p - p_N\|^2_{V_0} \\
&\leq c_0^2 \frac{1}{N} \|y\|^2_{V_1} + \lambda^{-1} c_0^2 \frac{1}{N} \|p\|^2_{V_1} = c_0^2 \frac{1}{N} \|(y,p)\|^2_{P_1},
\end{aligned}$$

hence $\|(y,p) - (y_N, p_N)\|_{P_0} \leq c_0 (1/\sqrt{N}) \|(y,p)\|_{P_1}$. □

5.2. **Discretization error in h.** The discretization error between the multiharmonic approximation of the exact solution and its multiharmonic finite element approximation can be deduced to the discretization error between the unknown Fourier coefficients and their finite element approximations, see [20]. We have that

$$\begin{aligned}
\|(y_N, p_N) - (y_{Nh}, p_{Nh})\|^2_{P_0} &= T \|(y_0^c, p_0^c) - (y_{0h}^c, p_{0h}^c)\|^2_P \\
&\quad + \frac{T}{2} \sum_{k=1}^{N} \|(\boldsymbol{y}_k, \boldsymbol{p}_k) - (\boldsymbol{y}_{kh}, \boldsymbol{p}_{kh})\|^2_{\mathcal{P}}.
\end{aligned}$$

The following theorem provides an estimate for discretization error between the unknown Fourier coefficients and their finite element approximations:

Theorem 6. *Under the assumption that $(\boldsymbol{y}_k, \boldsymbol{p}_k) \in (H^2(\Omega))^4$ the discretization error for the Fourier coefficients can be estimated by*

$$\|(\boldsymbol{y}_k, \boldsymbol{p}_k) - (\boldsymbol{y}_{kh}, \boldsymbol{p}_{kh})\|_{\mathcal{P}} \leq c_1 c_{par}(\lambda, k, \omega, \overline{\nu}, \overline{\sigma}, h)\, h\, |(\boldsymbol{y}_k, \boldsymbol{p}_k)|_{H^2(\Omega)}, \tag{47}$$

where c_1 is a positive constant and $c_{par}^2(\lambda,k,\omega,\overline{\nu},\overline{\sigma},h) = \sqrt{\lambda}\overline{\nu}c_{1,2}^2+(1+k\omega\sqrt{\lambda}\overline{\sigma})c_{0,2}^2h^2$ with constants $c_{0,2}$ and $c_{1,2}$ from the approximation theorem, and $|\cdot|_{H^2(\Omega)}$ is a weighted $H^2(\Omega)$-seminorm defined by the relation

$$|(\boldsymbol{y}_k,\boldsymbol{p}_k)|_{H^2(\Omega)}^2 = |\boldsymbol{y}_k|_{H^2(\Omega)}^2 + \lambda^{-1}|\boldsymbol{p}_k|_{H^2(\Omega)}^2.$$

Proof. See [20]. □

The following theorem provides the estimate for the complete discretization error in h:

Theorem 7. *Under the assumptions of Theorem 6, the discretization error in h can be estimated as follows:*

$$\|(y_N,p_N)-(y_{Nh},p_{Nh})\|_{P_0} \le c_1\, c_{par}(\lambda,N,\omega,\overline{\nu},\overline{\sigma},h)\, h\, |(y_N,p_N)|_{H^2}, \tag{48}$$

where $c_{par}^2(\lambda,N,\omega,\overline{\nu},\overline{\sigma},h) = \sqrt{\lambda}\overline{\nu}c_{1,2}^2 + (1+N\omega\sqrt{\lambda}\overline{\sigma})c_{0,2}^2h^2$ with constants $c_{0,2}$ and $c_{1,2}$ from the approximation theorem and where the H^2-seminorm is given by

$$|(y_N,p_N)|_{H^2}^2 = T|(y_0^c,p_0^c)|_{H^2(\Omega)}^2 + \frac{T}{2}\sum_{k=1}^{N}|(\boldsymbol{y}_k,\boldsymbol{p}_k)|_{H^2(\Omega)}^2,$$

which is an $H^{2,0}(Q_T)$-seminorm defined in the Fourier space. The $H^2(\Omega)$-seminorm for the Fourier coefficients is given in Theorem 6.

Proof. The proof follows immediately from Theorem 6, see [20]. □

Remark 5. *As it has been mentioned in* [20]*, the convergence rate in (47), hence also in (48), reduces from h to h^s with some $s\in(0,1)$ if the Fourier coefficients of y and p only belong to $H^{1+s}(\Omega)$. This result can be proven with the help of space interpolation theory, see* [2, 8].

5.3. **Complete discretization error.** We have to introduce new function spaces and corresponding norms such that we can estimate both, the P_1-norm of the discretization error in Theorem 5 and the H^2-seminorm of the discretization error in Theorem 7, by one norm.

Definition 4. *We define the following function spaces:*

$$\begin{aligned}(H^{0,\frac{1}{2}})^2 &:= \{v\in H^{0,\frac{1}{2}} : \nabla v, \nabla^2 v \in H^{0,\frac{1}{2}}\},\\ (H_{per}^{0,1})^1 &:= \{v\in H_{per}^{0,1} : \nabla v \in H_{per}^{0,1}\},\\ X &:= (H^{0,\frac{1}{2}})^2 \cap (H_{per}^{0,1})^1,\end{aligned}$$

where we define the following norm in the space X:

$$\begin{aligned}\|y\|_X^2 &= \|y\|_{L^2(Q_T)}^2 + \left\|\partial_t^{1/2}y\right\|_{L^2(\Omega)}^2 + \left\|\partial_t y\right\|_{L^2(Q_T)}^2 + \|\nabla y\|_{L^2(Q_T)}^2\\ &\quad + \left\|\partial_t^{1/2}\nabla y\right\|_{L^2(Q_T)}^2 + \left\|\partial_t\nabla y\right\|_{L^2(Q_T)}^2 + \|\nabla^2 y\|_{L^2(Q_T)}^2 + \left\|\partial_t^{1/2}\nabla^2 y\right\|_{L^2(Q_T)}^2\end{aligned}$$

defined in the Fourier space according to Definition 2, i.e.

$$\begin{aligned}\|y\|_X^2 &= T(\|y_0^c\|_{L^2(\Omega)}^2 + \|\nabla y_0^c\|_{L^2(\Omega)}^2 + \|\nabla^2 y_0^c\|_{L^2(\Omega)}^2)\\ &\quad + \frac{T}{2}\sum_{k=1}^{\infty}[(1+k\omega+(k\omega)^2)\|\boldsymbol{y}_k\|_{L^2(\Omega)}^2\\ &\quad + (1+k\omega+(k\omega)^2)\|\nabla\boldsymbol{y}_k\|_{L^2(\Omega)}^2 + (1+k\omega)\|\nabla^2\boldsymbol{y}_k\|_{L^2(\Omega)}^2].\end{aligned}$$

Moreover, we define the following vector-valued norm:

$$\|(y,p)\|_X^2 = \|y\|_X^2 + \lambda^{-1}\|p\|_X^2.$$

Remark 6. *The H^2-seminorm of the space $H^{2,0}(Q_T)$ defined in Theorem 7 is bounded by the X-norm, i.e.*

$$|y|_{H^2} = T|y_0^c|^2_{H^2(\Omega)} + \frac{T}{2}\sum_{k=1}^{\infty}|\boldsymbol{y}_k|^2_{H^2(\Omega)} \leq \|y\|^2_X.$$

The same bound is valid for the vector-valued versions of the H^2-seminorm and the X-norm as well.

The following lemma shows that the V_1-norm and the P_1-norm are also bounded by the X-norm and the vector-valued X-norm, respectively.

Lemma 2. *The P_1-norm is bounded by the vector-valued X-norm, i.e.*

$$\|(y,p)\|_{P_1} \leq c\|(y,p)\|_X \tag{49}$$

with the constant $c^2 = \max\{1, \sqrt{\lambda}\overline{\nu}, \sqrt{\lambda}\overline{\sigma}\}$.

Proof. We have that

$$\begin{aligned}
\|y\|^2_{V_1} &= T(\|y_0^c\|^2_{L^2(\Omega)} + \sqrt{\lambda}(\nu\nabla y_0^c, \nabla y_0^c)_{L^2(\Omega)}) \\
&\quad + \frac{T}{2}\sum_{k=1}^{\infty}[(1+k\omega)\|\boldsymbol{y}_k\|^2_{L^2(\Omega)} + \sqrt{\lambda}(1+k\omega)(\nu\nabla\boldsymbol{y}_k, \nabla\boldsymbol{y}_k)_{L^2(\Omega)} \\
&\quad + \sqrt{\lambda}(k\omega)^2(\sigma\boldsymbol{y}_k, \boldsymbol{y}_k)_{L^2(\Omega)}] \\
&\leq T(\|y_0^c\|^2_{L^2(\Omega)} + \sqrt{\lambda}\overline{\nu}\|\nabla y_0^c\|^2_{L^2(\Omega)}) \\
&\quad + \frac{T}{2}\sum_{k=1}^{\infty}[(1+k\omega+\sqrt{\lambda}\overline{\sigma}(k\omega)^2)\|\boldsymbol{y}_k\|^2_{L^2(\Omega)} + \sqrt{\lambda}\overline{\nu}(1+k\omega)\|\nabla\boldsymbol{y}_k\|^2_{L^2(\Omega)}] \\
&\leq \max\{1, \sqrt{\lambda}\overline{\nu}, \sqrt{\lambda}\overline{\sigma}\}\Big(T(\|y_0^c\|^2_{L^2(\Omega)} + \|\nabla y_0^c\|^2_{L^2(\Omega)}) \\
&\quad + \frac{T}{2}\sum_{k=1}^{\infty}[(1+k\omega+(k\omega)^2)\|\boldsymbol{y}_k\|^2_{L^2(\Omega)} + (1+k\omega)\|\nabla\boldsymbol{y}_k\|^2_{L^2(\Omega)}]\Big) \\
&\leq \max\{1, \sqrt{\lambda}\overline{\nu}, \sqrt{\lambda}\overline{\sigma}\}\Big(T(\|y_0^c\|^2_{L^2(\Omega)} + \|\nabla y_0^c\|^2_{L^2(\Omega)} + \|\nabla^2 y_0^c\|^2_{L^2(\Omega)}) \\
&\quad + \frac{T}{2}\sum_{k=1}^{\infty}[(1+k\omega+(k\omega)^2)\|\boldsymbol{y}_k\|^2_{L^2(\Omega)} + (1+k\omega+(k\omega)^2)\|\nabla\boldsymbol{y}_k\|^2_{L^2(\Omega)} \\
&\quad + (1+k\omega)\|\nabla^2\boldsymbol{y}_k\|^2_{L^2(\Omega)}]\Big) = c^2\|y\|^2_X
\end{aligned}$$

with $c^2 = \max\{1, \sqrt{\lambda}\overline{\nu}, \sqrt{\lambda}\overline{\sigma}\}$. □

Now we can estimate the complete error arising from the multiharmonic finite element discretization.

Theorem 8. *Let us assume that $y, p \in X$. Then the complete discretization error arising from the multiharmonic finite element discretization can be estimated by*

$$\|(y,p) - (y_{Nh}, p_{Nh})\|_{P_0} \leq C\Big(\frac{1}{\sqrt{N}} + c_{par}(\lambda, N, \omega, \overline{\nu}, \overline{\sigma}, h)\, h\Big)\, \|(y,p)\|_X, \tag{50}$$

where $C = c\max\{c_0, c_1\}$ with c_0, c_1 and c from Theorem 5, Theorem 7 and Lemma 2, respectively, and $c^2_{par}(\lambda, N, \omega, \overline{\nu}, \overline{\sigma}, h) = \sqrt{\lambda}\overline{\nu}c^2_{1,2} + (1+N\omega\sqrt{\lambda}\overline{\sigma})c^2_{0,2}h^2$ with constants $c_{0,2}$ and $c_{1,2}$ from the approximation theorem.

Proof. Applying triangle inequality and Theorems 5, 6 and 7 yields

$$\begin{aligned}\|(y,p)-(y_{Nh},p_{Nh})\|_{P_0} &\le \|(y,p)-(y_N,p_N)\|_{P_0} + \|(y_N,p_N)-(y_{Nh},p_{Nh})\|_{P_0}\\ &\le c_0\frac{1}{\sqrt{N}}\|(y,p)\|_{P_1} + c_1\, c_{par}(\lambda,N,\omega,\overline{\nu},\overline{\sigma},h)\, h\,|(y_N,p_N)|_{H^2}\\ &\le \max\{c_0,c_1\}\Big(\frac{1}{\sqrt{N}}\|(y,p)\|_{P_1} + c_{par}(\lambda,N,\omega,\overline{\nu},\overline{\sigma},h)\, h\,|(y_N,p_N)|_{H^2}\Big).\end{aligned}$$

From Lemma 2 and Remark 6 follows that

$$\begin{aligned}\|(y,p)-(y_{Nh},p_{Nh})\|_{P_0} &\le c\max\{c_0,c_1\}\Big(\frac{1}{\sqrt{N}}\|(y,p)\|_X\\ &\quad + c_{par}(\lambda,N,\omega,\overline{\nu},\overline{\sigma},h)\, h\,\|(y_N,p_N)\|_X\Big)\\ &\le C\Big(\frac{1}{\sqrt{N}} + c_{par}(\lambda,N,\omega,\overline{\nu},\overline{\sigma},h)\, h\Big)\,\|(y,p)\|_X\end{aligned}$$

with the constant $C = c\max\{c_0,c_1\}$. □

Remark 7. *From Theorem 8 we observe a relation between the discretization parameters N and h: in the case of having a low regularity assumption, we have to choose $N = \mathcal{O}(h^{-2})$ in order to get a good bound for the complete discretization error.*

6. Numerical Results

In this section, we present and discuss the results of our numerical experiments, where we study the numerical behavior of our multiharmonic finite element method. More precisely, we investigate the practical convergence behavior with respect to the space and time discretizations as well as the efficiency and the robustness of our preconditioned MINRES solver in different settings. We use the AMLI preconditioner proposed by Kraus in [24] for an inexact realization of our block-diagonal preconditioner in the MINRES method. First numerical results with this AMLI preconditioner in the context of multiharmonic parabolic optimal control problems were presented in [20], where the authors considered an optimal control problem with a given time-harmonic desired state. In this paper, we present new numerical results for the following more general settings:

1. the desired state is zero, and there is a given time-harmonic source term in the PDE constraints,
2. the desired state is periodic and analytic in time,
3. the desired state is analytic in time, but not time-periodic,
4. the desired state is a characteristic function in space and time, and
5. the desired state is a characteristic function in space and time, but in addition, there are jumps in ν and σ.

We mention that the desired state is unreachable in Examples 3, 4 and 5. We consider our optimal control problem (1)-(3), where the computational domain $\Omega = (0,1)\times(0,1)$ is uniformly decomposed into triangles, and standard continuous, piecewise linear finite elements are used for the discretization in space. The material coefficients are supposed to be piecewise constant on Ω. In Examples 1, 2, 3 and 4, we set $\sigma = \nu = 1$, but in Example 5, we consider jumping material coefficients. The desired states in Examples 2, 3, 4 and 5 are not time-harmonic. Therefore, we have to compute their Fourier coefficients for different modes k in order to expand the desired states into truncated Fourier series. The Examples 1 and 4 have been taken from [1], but with homogeneous Dirichlet boundary conditions instead of Robin conditions. We mention that, in all tables where the number of MINRES iterations is presented, the iteration was stopped after reducing the residual by a factor of 10^{-6}. In each MINRES iteration step, we have used the AMLI preconditioner

according to [24] with 2 inner iterations. The computations for the figures of all examples were obtained on a 64×64-grid. The results on grids of smaller mesh sizes were very similar. All computations were performed on a PC with Intel(R) Core(TM) i7-2600 CPU @3.40 GHz.

In the **first example**, the desired state y_d is set 0, and the nontrivial time-harmonic source term

$$f(\boldsymbol{x},t) = x_1^2(1-x_1)^2 x_2^2(1-x_2)^2 \sin(2\pi t)$$

is given. The frequency is set $\omega = 2\pi$. Hence, we have the time period $T = 1$. This leads now to the following new Lagrange functional of our minimization problem:

$$\mathcal{L}(y,u,p) := \mathcal{J}(y,u) - \int_0^T \int_\Omega \Big(\sigma \frac{\partial y}{\partial t} - \nabla \cdot \big(\nu \nabla y\big) - u - f\Big) p \, d\boldsymbol{x} \, dt. \tag{51}$$

Finally, the optimality conditions (16) yield the following reduced optimality system written in its classical formulation as

$$\begin{cases} \sigma(\boldsymbol{x}) \dfrac{\partial}{\partial t} y(\boldsymbol{x},t) - \nabla \cdot (\nu(\boldsymbol{x}) \nabla y(\boldsymbol{x},t)) + \lambda^{-1} p(\boldsymbol{x},t) = f(\boldsymbol{x},t), & (\boldsymbol{x},t) \in Q_T, \\ y(\boldsymbol{x},t) = 0, & (\boldsymbol{x},t) \in \Sigma_T, \\ y(\boldsymbol{x},0) = y(\boldsymbol{x},T), & \boldsymbol{x} \in \Omega, \\ -\sigma(\boldsymbol{x}) \dfrac{\partial}{\partial t} p(\boldsymbol{x},t) - \nabla \cdot (\nu(\boldsymbol{x}) \nabla p(\boldsymbol{x},t)) - y(\boldsymbol{x},t) = 0, & (\boldsymbol{x},t) \in Q_T, \\ p(\boldsymbol{x},t) = 0, & (\boldsymbol{x},t) \in \Sigma_T, \\ p(\boldsymbol{x},T) = p(\boldsymbol{x},0), & \boldsymbol{x} \in \Omega. \end{cases} \tag{52}$$

The space-time variational formulation of (52) is obtained in the same way as for (18) in Subsection 2.2, and can be written in the following way: Given the source term $f \in L^2(Q_T)$, find y and p from $H_0^{1,\frac{1}{2}}(Q_T)$ such that

$$\begin{cases} \displaystyle\int_{Q_T} \Big(y\, v - \nu(\boldsymbol{x}) \nabla p \cdot \nabla v + \sigma(\boldsymbol{x}) \frac{\partial^{1/2} p}{\partial t^{1/2}} \frac{\partial^{1/2} v^\perp}{\partial t^{1/2}} \Big) \, d\boldsymbol{x} \, dt = 0, \\ \displaystyle\int_{Q_T} \Big(\nu(\boldsymbol{x}) \nabla y \cdot \nabla q + \sigma(\boldsymbol{x}) \frac{\partial^{1/2} y}{\partial t^{1/2}} \frac{\partial^{1/2} q^\perp}{\partial t^{1/2}} + \lambda^{-1} p\, q \Big) \, d\boldsymbol{x} \, dt = \int_{Q_T} f\, v \, d\boldsymbol{x} \, dt \end{cases} \tag{53}$$

for all test functions $v, q \in H_0^{1,\frac{1}{2}}(Q_T)$, where all functions are given in their Fourier series expansion in time according to Definition 2. We discretize the variational problem (53) by means of the multiharmonic finite element method. Since the source term is time-harmonic, we obtain the following linear system for $k = 1$ only:

$$\begin{pmatrix} M_h & 0 & -K_h & \omega M_{h,\sigma} \\ 0 & M_h & -\omega M_{h,\sigma} & -K_h \\ -K_h & -\omega M_{h,\sigma} & -\lambda^{-1} M_h & 0 \\ \omega M_{h,\sigma} & -K_h & 0 & -\lambda^{-1} M_h \end{pmatrix} \begin{pmatrix} \underline{y}^c \\ \underline{y}^s \\ \underline{p}^c \\ \underline{p}^s \end{pmatrix} = \begin{pmatrix} 0 \\ 0 \\ \underline{f}^c \\ \underline{f}^s \end{pmatrix}, \tag{54}$$

where $\underline{f}^c = 0$ since the source term is only sine-wave-excited. As we see, only the right hand side of the optimality system and hence of the corresponding discretized system has changed. So, we can solve our problem in the same way as before and can use the same AMLI preconditioner as proposed in Section 4. Table 1 and Table 2 present the number of MINRES iterations and the computational times in seconds, respectively, varying the values of the parameter λ on grids of different mesh sizes. In Figure 1, we illustrate the harmonic source term and the finite element approximations of the control for different values of λ, more precisely, for $\lambda \in \{1, 10^{-2}, 10^{-4}, 10^{-6}\}$. Figure 2 presents the finite element approximations to the state for the same different values of λ. Both figures demonstrate that, for λ approaching 0, the control and the state approach the harmonic source term and the desired state, respectively. Compared to the methods used in [1], where the authors

observe that the convergence of their nested multigrid method is strongly affected by the regularization parameter λ, the convergence of our AMLI preconditioned MINRES solver is robust with respect to the regularization parameter λ and has optimal complexity at the same time, cf. Tables 1 and 2.

n_{iter}	λ								
grid	10^{-8}	10^{-6}	10^{-4}	10^{-2}	1	10^{2}	10^{4}	10^{6}	10^{8}
64×64	9	10	12	10	10	12	14	16	18
128×128	9	11	12	10	12	12	14	17	18
256×256	9	12	14	12	12	12	14	18	20
512×512	9	12	14	12	12	14	14	16	18

TABLE 1. Number of MINRES iterations n_{iter} for different values of λ on grids of different mesh size (Example 1)

time (in s)	λ								
grid	10^{-8}	10^{-6}	10^{-4}	10^{-2}	1	10^{2}	10^{4}	10^{6}	10^{8}
64×64	0.09	0.10	0.12	0.10	0.10	0.12	0.14	0.15	0.17
128×128	0.44	0.54	0.60	0.49	0.61	0.58	0.70	0.83	0.89
256×256	1.99	2.64	3.09	2.66	2.66	2.65	3.09	3.95	4.39
512×512	8.50	11.32	13.21	11.35	11.30	13.19	13.22	15.02	16.87

TABLE 2. The computational times in seconds for different values of λ on grids of different mesh size (Example 1)

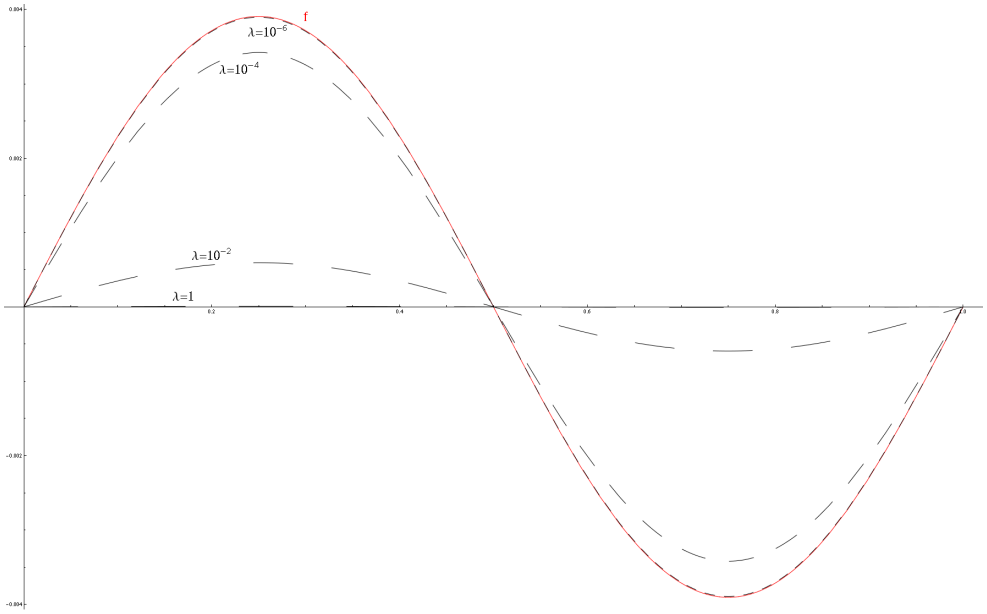

FIGURE 1. The harmonic source term f (red) and the finite element approximations u_h to the control u for $\lambda = 1, 10^{-2}, 10^{-4}, 10^{-6}$ as functions of time in $[0, 1]$ at the spatial coordinates $(0.5, 0.5)$ and for $\omega = 2\pi$ and $\sigma = \nu = 1$ (Example 1).

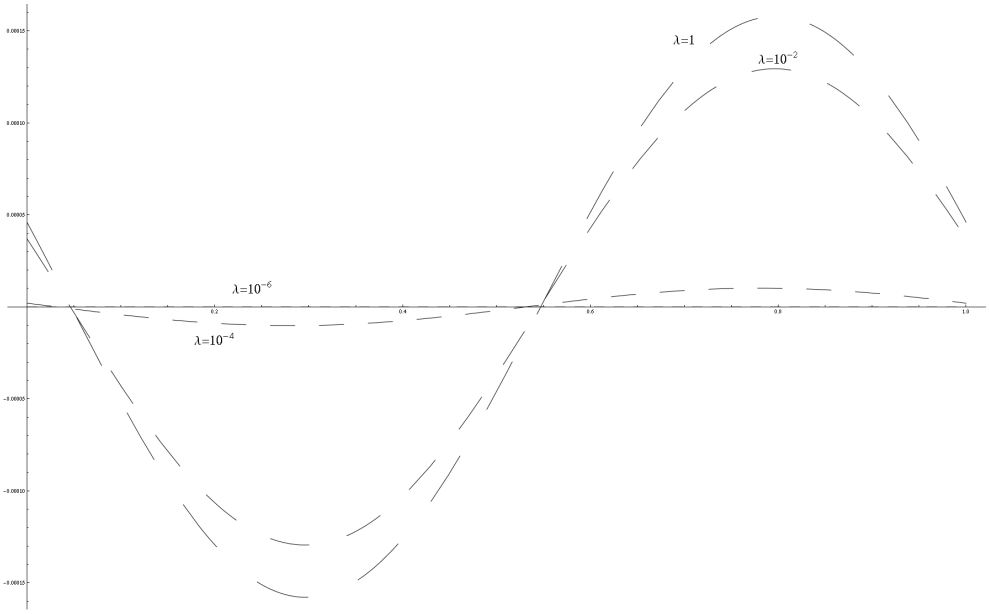

FIGURE 2. The finite element approximations y_h to the state y for $\lambda = 1, 10^{-2}, 10^{-4}, 10^{-6}$ as functions of time in $[0,1]$ at the spatial coordinates $(0.5, 0.5)$ and for $\omega = 2\pi$ and $\sigma = \nu = 1$ (Example 1).

In the **second example**, we consider a given time-periodic and analytic, but not time-harmonic, desired state of the form

$$y_d(\boldsymbol{x},t) = e^t \sin(t)\left(\left(3+4\pi^4\right)\sin^2(t) - 6\cos^2(t) - 6\sin(t)\cos(t)\right)\sin(x_1\pi)\sin(x_2\pi),$$

where $T = \frac{2\pi}{\omega}$ with $\omega = 1$. We compute the Fourier series expansion in time of the desired state, i.e.

$$y_d(\boldsymbol{x},t) = y_{d0}^c(\boldsymbol{x}) + \sum_{k=1}^{\infty}\left(y_{dk}^c(\boldsymbol{x})\cos(k\omega t) + y_{dk}^s(\boldsymbol{x})\sin(k\omega t)\right)$$

with the Fourier coefficients

$$y_{dk}^c(\boldsymbol{x}) = \frac{2}{T}\int_0^T y_d(\boldsymbol{x},t)\cos(k\omega t)\,dt \quad \text{and} \quad y_{dk}^s(\boldsymbol{x}) = \frac{2}{T}\int_0^T y_d(\boldsymbol{x},t)\sin(k\omega t)\,dt,$$

which can here be computed analytically. We truncate the Fourier series and approximate the Fourier coefficients by finite element functions as it was presented in Section 3. Finally, we solve the systems (25) and (27) for all $0 \le k \le N$. Figure 3 illustrates the convergence of the multiharmonic finite element approximation to the exact solution for increasing N, where we set $\lambda = 1$. We have computed the multiharmonic finite element solutions for all modes up to $N = 5$, which provide already a very good approximation to the exact solution. The exact solution is given by

$$y(\boldsymbol{x},t) = e^t \sin(t)^3 \sin(x_1\pi)\sin(x_2\pi)$$

for $\lambda = 1$. In Figure 3, we observe the fast convergence of the multiharmonic finite element approximations y_{Nh} to the exact solution y at the spatial coordinates $(0.5, 0.5)$ and for $t \in [0,T]$, where the exact solution is given by

$$y(0.5, 0.5, t) = e^t \sin(t)^3.$$

In Figure 4, we illustrate the exact desired state y_d and the multiharmonic finite element approximations y_{Nh} to the state y for different values of λ, more precisely,

for $\lambda \in \{1, 10^{-2}, 10^{-4}, 10^{-6}\}$, as functions of time in $[0, T]$ at the spatial coordinates $\boldsymbol{x} = (0.5, 0.5)$ and for $N = 5$. Figure 5 presents the corresponding controls u_{Nh}.

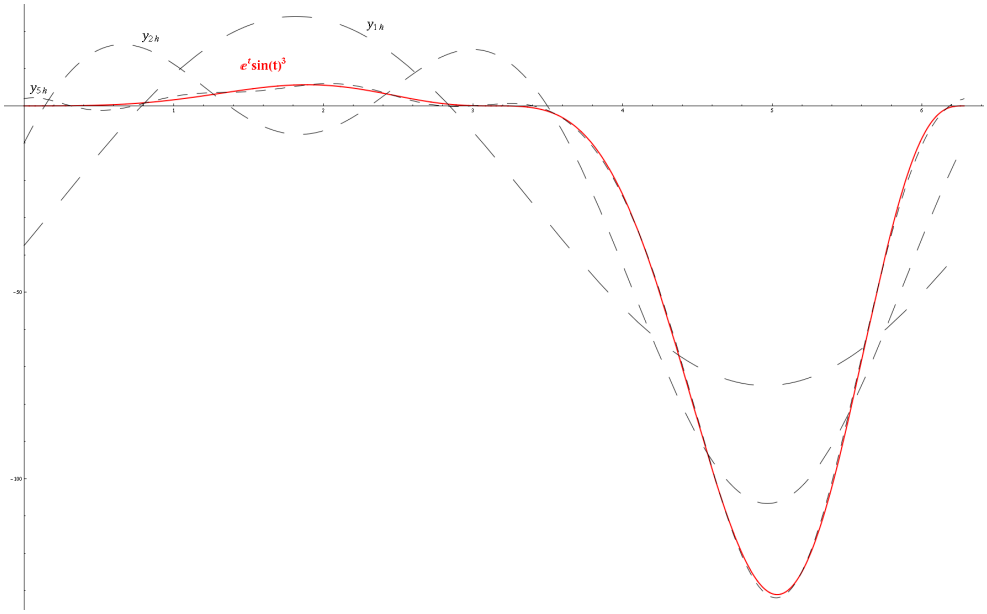

FIGURE 3. The exact state y (red) and its multiharmonic finite element approximations y_{Nh} for $N = 1, 2, 5$ as functions of time in $[0, 2\pi]$ at the spatial coordinates $(0.5, 0.5)$ and for $\lambda = 1$, $\omega = 1$ and $\sigma = \nu = 1$ (Example 2).

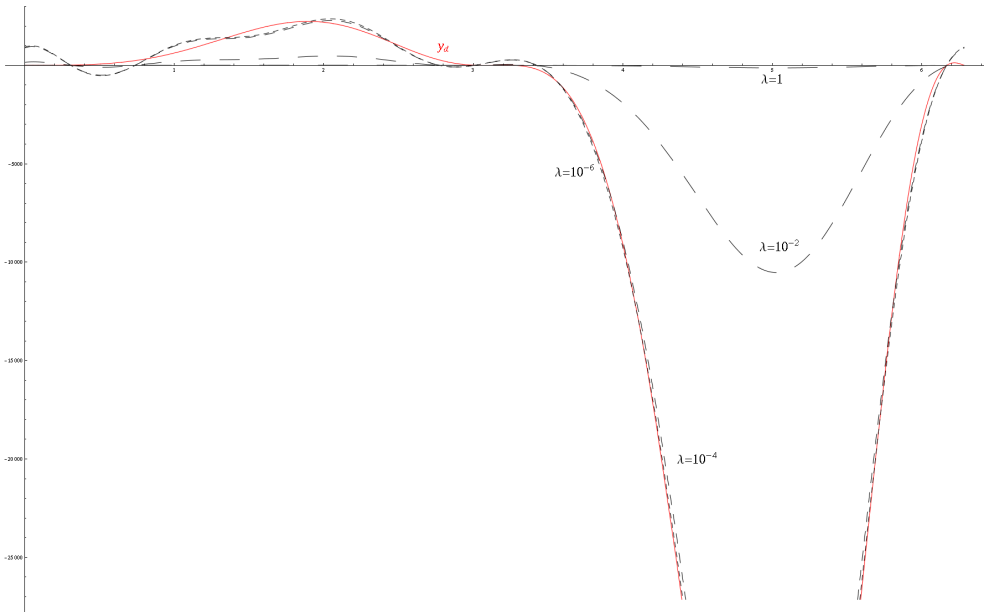

FIGURE 4. The desired state y_d (red) and the multiharmonic finite element approximation of the solution y_{Nh} with $N = 5$ for $\lambda = 1, 10^{-2}, 10^{-4}, 10^{-6}$ as functions of time in $[0, 2\pi]$ at the spatial coordinates $(0.5, 0.5)$ and for $\omega = 1$ and $\nu = \sigma = 1$ (Example 2).

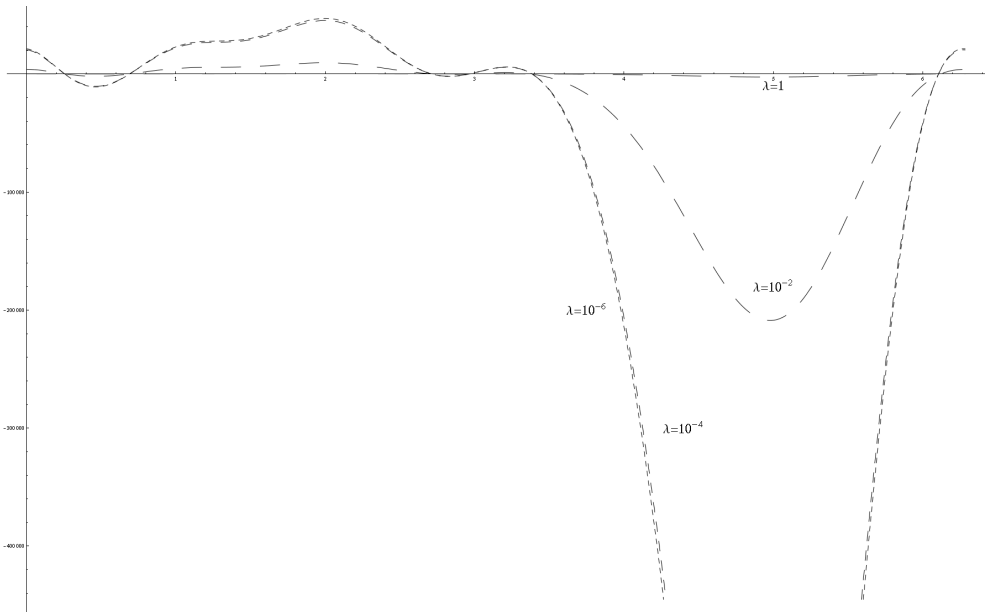

FIGURE 5. The multiharmonic finite element approximations u_{Nh} to the control u with $N = 5$ for $\lambda = 1, 10^{-2}, 10^{-4}, 10^{-6}$ as functions of time in $[0, 2\pi]$ at the spatial coordinates $(0.5, 0.5)$ and for $\omega = 1$ and $\sigma = \nu = 1$ (Example 2).

Table 3 presents the iteration numbers, and Table 4 the computational times for the mode $k = 1$ obtained on grids of different mesh sizes. We present the iteration numbers and the computational times only for $k = 1$ because the computations of all modes up to the truncation index N can be done totally in parallel and lead to similar results.

n_{iter}	λ								
grid	10^{-8}	10^{-6}	10^{-4}	10^{-2}	1	10^{2}	10^{4}	10^{6}	10^{8}
64×64	19	16	14	12	12	12	12	12	12
128×128	18	16	14	12	14	13	14	14	14
256×256	18	16	14	13	16	17	15	15	15
512×512	18	17	14	16	18	21	41	35	33

TABLE 3. Number of MINRES iterations n_{iter} for different values of λ on grids of different mesh size (Example 2)

time (in s)	λ								
grid	10^{-8}	10^{-6}	10^{-4}	10^{-2}	1	10^{2}	10^{4}	10^{6}	10^{8}
64×64	0.19	0.16	0.14	0.12	0.12	0.12	0.13	0.12	0.13
128×128	0.88	0.80	0.71	0.59	0.69	0.64	0.70	0.70	0.70
256×256	4.02	3.59	3.15	2.93	3.61	3.80	3.37	3.38	3.37
512×512	17.20	16.29	13.51	15.38	17.34	20.02	38.53	33.08	31.16

TABLE 4. The computational times in seconds for different values of λ on grids of different mesh size (Example 2)

Altogether, Figure 3, Figure 4 and Figure 5 as well as Table 3 and Table 4 confirm that the multiharmonic finite element method is a very efficient approach for solving

time-periodic problems. In the following, we will consider an example, where the desired state is not time-periodic anymore.

In the **third example**, we choose the time-analytic desired state

$$y_d(\boldsymbol{x}, t) = e^t(-2\cos(t) + \sin(t) + 4\pi^4 \sin(t)) \sin(x_1\pi) \sin(x_2\pi),$$

which is obviously not time-periodic. We set again $\omega = 1$. Hence, the time-period $T = 2\pi/\omega$ is equal to 2π. For this example, we compute the Fourier coefficients of the desired state again analytically. In Figure 6, we present the exact state y and its multiharmonic finite element approximations y_{Nh} with $N = 1, 2, 5$ as functions of time in $[0, T]$ at the spatial coordinates $(0.5, 0.5)$ and for the parameter choice $\lambda = 1$. In this case, the exact state is given by

$$y(0.5, 0.5, t) = e^t \sin(t).$$

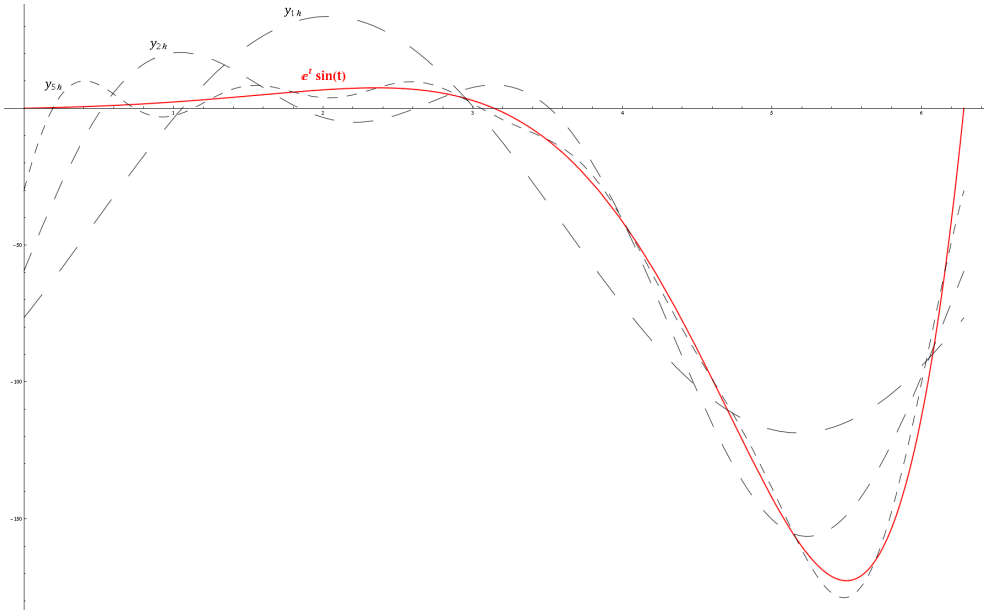

FIGURE 6. The exact state y (red) and its multiharmonic finite element approximations y_{Nh} with $N = 1, 2, 5$ as functions of time in $[0, 2\pi]$ at the spatial coordinates $(0.5, 0.5)$ and for $\lambda = 1$ and $\sigma = \nu = 1$ (Example 3).

As for the previous two examples, we illustrate in Figure 7 how the multiharmonic finite element approximations y_{5h} of the state y approach the desired state y_d as λ goes to zero. Figure 8 shows the corresponding controls u_{5h} for the same different values of λ as in Figure 7.

In Table 5 and Table 6, we present some numerical results for Example 3 on grids of different mesh size, where we set $k = 1$ and varying the cost parameter λ.

In the **fourth example**, we consider the desired state

$$y_d(\boldsymbol{x}, t) = \chi_{[\frac{1}{4}, \frac{3}{4}]}(t) \chi_{[\frac{1}{2}, 1]^2}(\boldsymbol{x}),$$

that is a characteristic function in space and time. The time period is set $T = 1$, hence $\omega = 2\pi$. We can compute the Fourier coeffcients of our Fourier series

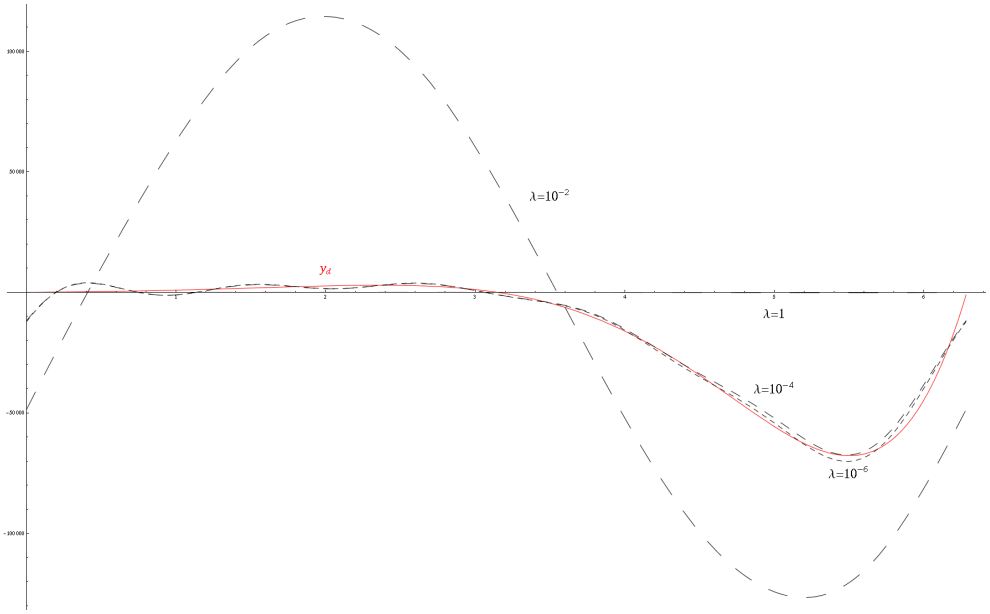

FIGURE 7. The desired state y_d (red) and the multiharmonic finite element approximation y_{Nh} of the state y with $N = 5$ for $\lambda = 1, 10^{-2}, 10^{-4}, 10^{-6}$ as functions of time in $[0, 2\pi]$ at the spatial coordinates $(0.5, 0.5)$ and for $\omega = 1$ and $\nu = \sigma = 1$ (Example 3).

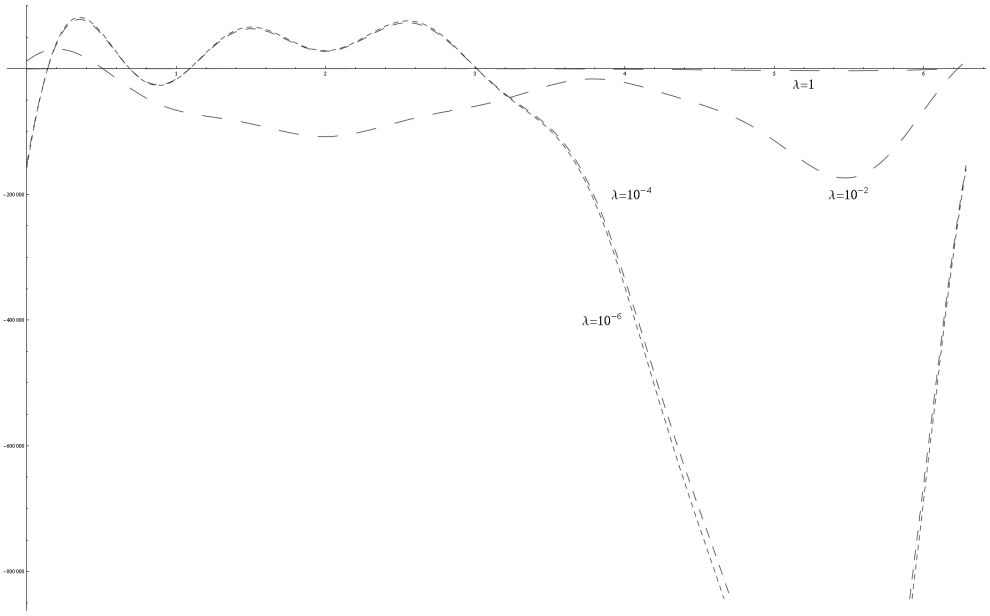

FIGURE 8. The multiharmonic finite element approximations of the control u_{Nh} with $N = 5$ for $\lambda = 1, 10^{-2}, 10^{-4}, 10^{-6}$ as functions of time in $[0, 2\pi]$ for the spatial coordinates $(0.5, 0.5)$ and with $\omega = 1$ and $\sigma = \nu = 1$ (Example 3).

expansion of the desired state again analytically, i.e.

$$y_{dk}^c(\boldsymbol{x}) = \frac{2}{T}\int_0^T y_d(\boldsymbol{x},t)\cos(k\omega t)\,dt = 2\int_0^1 \chi_{[\frac{1}{4},\frac{3}{4}]}(t)\chi_{[\frac{1}{2},1]^2}(\boldsymbol{x})\cos(2k\pi t)\,dt$$
$$= \chi_{[\frac{1}{2},1]^2}(\boldsymbol{x})\,2\int_{\frac{1}{4}}^{\frac{3}{4}}\cos(2k\pi t)\,dt = \chi_{[\frac{1}{2},1]^2}(\boldsymbol{x})\,\frac{-\sin(\frac{k\pi}{2})+\sin(\frac{3k\pi}{2})}{k\pi},$$

n_{iter}	λ								
grid	10^{-8}	10^{-6}	10^{-4}	10^{-2}	1	10^2	10^4	10^6	10^8
64×64	19	16	14	12	12	12	12	12	12
128×128	18	16	14	12	14	13	14	14	14
256×256	18	16	14	13	16	17	15	15	15
512×512	18	17	14	16	18	21	41	35	33

TABLE 5. Number of MINRES iterations n_{iter} for different values of λ on grids of different mesh size (Example 3)

time (in s)	λ								
grid	10^{-8}	10^{-6}	10^{-4}	10^{-2}	1	10^2	10^4	10^6	10^8
64×64	0.19	0.15	0.14	0.13	0.12	0.12	0.12	0.12	0.13
128×128	0.90	0.80	0.70	0.59	0.69	0.66	0.70	0.71	0.71
256×256	4.01	3.58	3.16	2.94	3.60	3.84	3.36	3.37	3.36
512×512	17.21	16.27	13.50	15.37	17.24	20.02	38.72	33.07	31.19

TABLE 6. The computational times in seconds for different values of λ on grids of different mesh size (Example 3)

and analogously we compute

$$y_{dk}^s(\boldsymbol{x}) = \frac{2}{T}\int_0^T y_d(\boldsymbol{x},t)\sin(k\omega t)\,dt = \chi_{[\frac{1}{2},1]^2}(\boldsymbol{x})\,\frac{2\sin(\frac{k\pi}{2})\sin(k\pi)}{k\pi},$$

yielding $y_{dk}^s(\boldsymbol{x}) = 0$ for all $k \in \mathbb{N}$. Figure 9 and Figure 10 present the multi-harmonic finite element approximations y_{5h} to the state y and the corresponding approximations u_{5h} to the control u as functions of time at the spatial coordinates $(0.5, 0.5)$, respectively. In Figure 11, we illustrate the approximations u_{Nh} to control u for $N = 5$ and $N = 11$, and for different spatial coordinates, more precisely, for $(0.25, 0.25)$, $(0.5, 0.5)$ and $(0.75, 0.75)$, where we set $\lambda = 0.01$ for all cases.

Finally, we present the number of MINRES iterations and the computational times in seconds varying the values of the regularization parameter λ on grids of different mesh size for $k = 1$ in Table 7 and Table 8, respectively.

n_{iter}	λ								
grid	10^{-8}	10^{-6}	10^{-4}	10^{-2}	1	10^2	10^4	10^6	10^8
64×64	22	20	18	18	12	10	10	10	10
128×128	22	20	20	18	12	10	10	10	10
256×256	22	22	20	18	14	12	12	12	12
512×512	23	22	22	20	14	12	12	12	12

TABLE 7. Number of MINRES iterations n_{iter} for different values of λ on grids of different mesh size (Example 4)

In the **fifth example**, we consider again a desired state which is a characteristic function in space and time, but in addition, we allow jumps in the values of the material coefficients ν and σ. More precisely, $\nu = 10^{-4}$ and $\sigma = 1$ on subdomain $\Omega_1 = (0,1)\times(0,\frac{1}{2})$, and $\nu = 10^4$ and $\sigma = 10^2$ on $\Omega_2 = \Omega\backslash\overline{\Omega}_1$. The time-period is set $T = 2\pi$, hence $\omega = 1$. We again vary the regularization parameter λ, and compute the solutions on grids of different mesh size. The following desired state is chosen:

$$y_d(\boldsymbol{x},t) = \chi_{[\frac{\pi}{2},\pi]}(t)\chi_{[\frac{1}{4},\frac{3}{4}]^2}(\boldsymbol{x}).$$

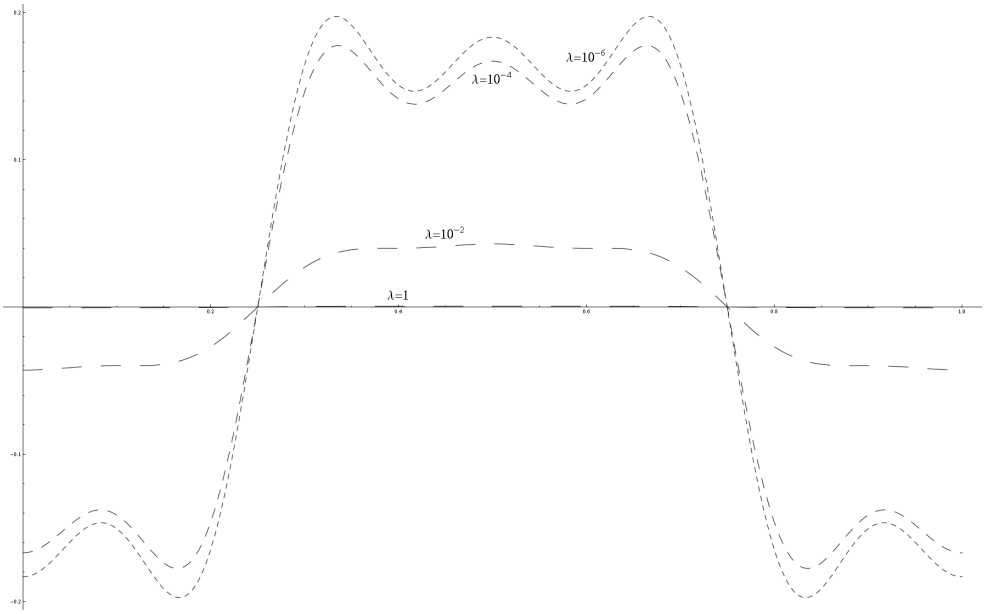

FIGURE 9. The multiharmonic finite element approximation y_{Nh} to the state y with $N = 5$ for $\lambda = 1, 10^{-2}, 10^{-4}, 10^{-6}$ as functions of time in $[0, 1]$ at the spatial coordinates $(0.5, 0.5)$, and for $\omega = 2\pi$ and $\nu = \sigma = 1$ (Example 4).

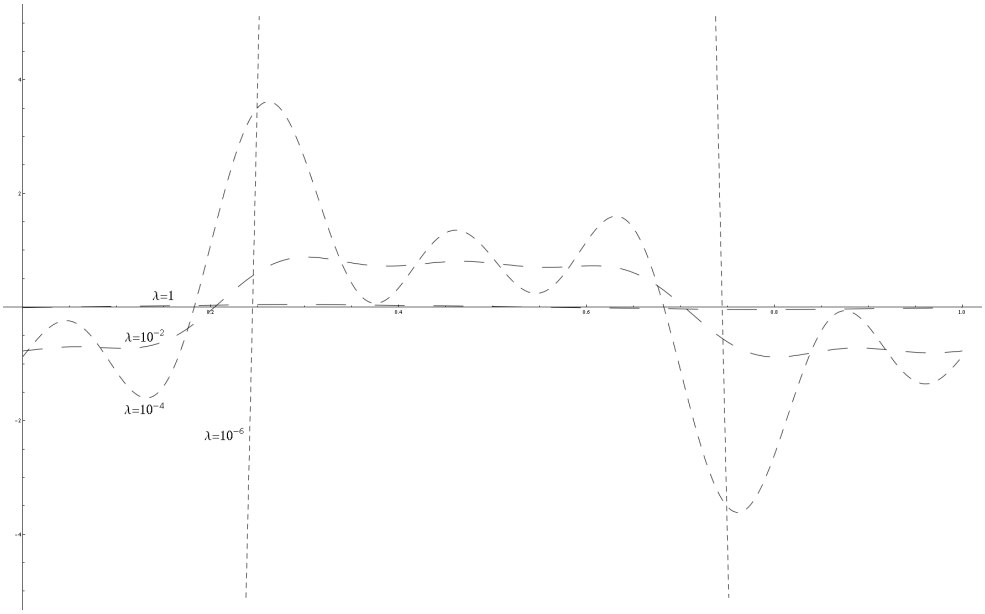

FIGURE 10. The multiharmonic finite element approximations u_{Nh} to the control u with $N = 5$ for $\lambda = 1, 10^{-2}, 10^{-4}, 10^{-6}$ as functions of time in $[0, 1]$ at the spatial coordinates $(0.5, 0.5)$, and for $\omega = 2\pi$ and $\sigma = \nu = 1$ (Example 4).

We again expand the desired state in a Fourier series, where the Fourier coeffcients can be computed analytically. We truncate then the Fourier series and approximate the Fourier coefficients by finite element functions. Finally, we solve the systems (25) and (27) for all $0 \le k \le N$.

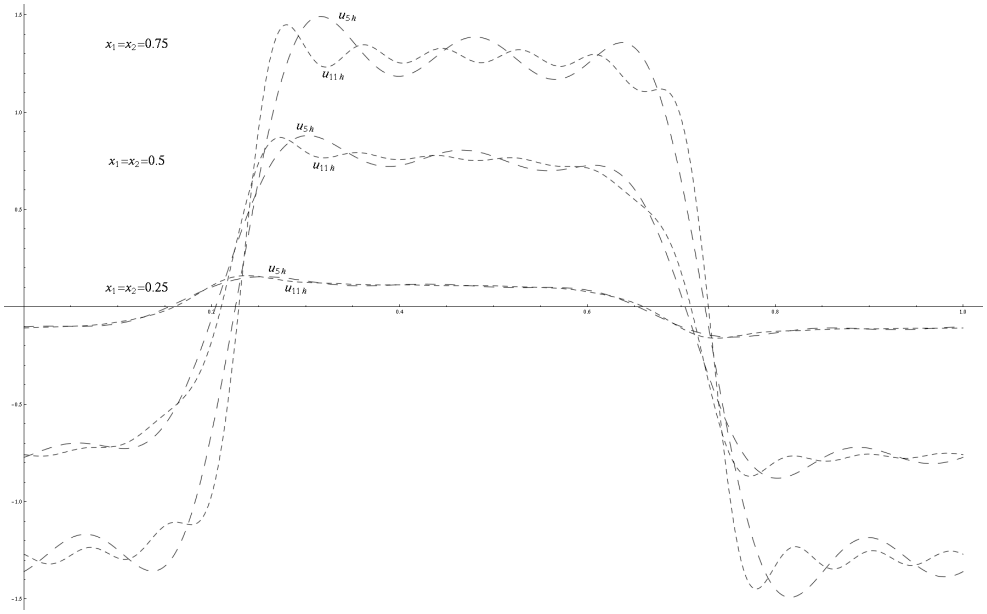

FIGURE 11. The multiharmonic finite element approximations u_{Nh} to the optimal control u with $N = 5$ and $N = 11$ at the spatial coordinates $(0.25, 0.25)$, $(0.5, 0.5)$ and $(0.75, 0.75)$ for $\lambda = 0.01$ as functions of time in $[0, 1]$ (Example 4).

time (in s)	λ								
	10^{-8}	10^{-6}	10^{-4}	10^{-2}	1	10^{2}	10^{4}	10^{6}	10^{8}
64×64-grid	0.21	0.20	0.18	0.18	0.11	0.10	0.10	0.10	0.10
128×128-grid	1.07	0.97	0.98	0.87	0.58	0.49	0.48	0.49	0.48
256×256-grid	4.80	4.80	4.37	3.93	3.06	2.62	2.63	2.65	2.65
512×512-grid	21.46	20.58	20.60	18.75	13.15	11.32	11.29	11.27	11.33

TABLE 8. The computational times in seconds for different values of λ on grids of different mesh size (Example 4)

In Figure 12 and Figure 13, we illustrate the multiharmonic finite element approximations y_{5h} to the state y and the corresponding approximations u_{5h} to the control u as functions of time at the spatial coordinates $(0.5, 0.5)$, respectively. Finally, the number of MINRES iterations and the corresponding computational times can be found in Table 9 and Table 10, respectively. We observe from these tables that our solver also remains robust with respect to both the regularization parameter λ and the mesh size h in case of large jumps in the values of the coefficient functions ν and σ. This is very important for many practical applications where we have usually large jumps in the values of material coefficients.

7. Conclusions and Outlook

In this paper, we have presented the multiharmonic finite element analysis of a time-periodic parabolic optimal control problem. We have first proved the existence and uniqueness of a special weak solution to the parabolic time-periodic boundary value problem that appears as PDE constraint in our optimal control problem. This result implies the unique solvability of our optimal control problem. Furthermore, we have studied the multiharmonic finite element method for solving

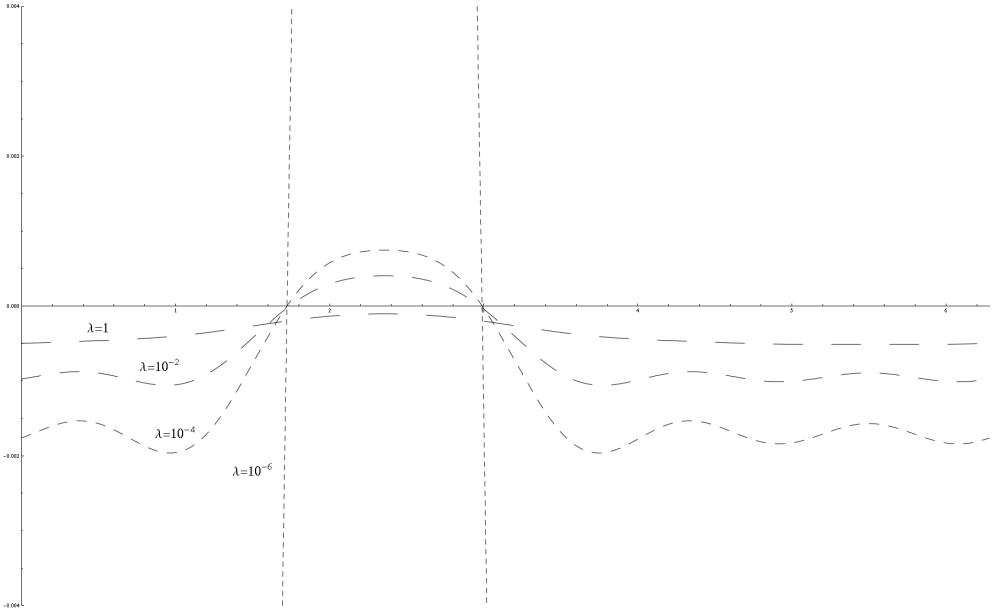

FIGURE 12. The multiharmonic finite element approximation y_{Nh} to the state y with $N = 5$ for $\lambda = 1, 10^{-2}, 10^{-4}, 10^{-6}$ as functions of time in $[0, 1]$ at the spatial coordinates $(0.5, 0.5)$ for $\omega = 1$ and with jumping material coefficients (Example 5).

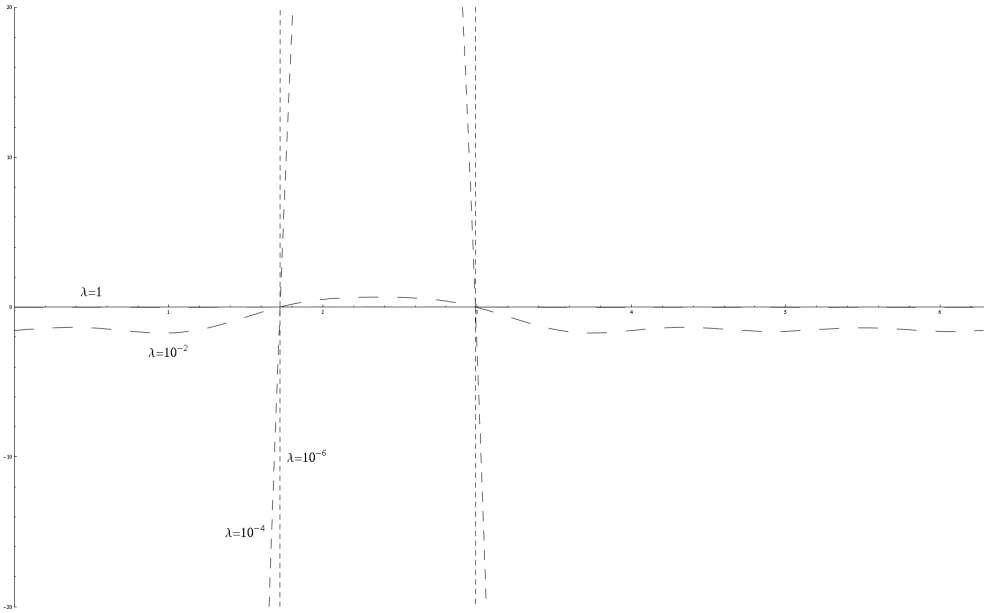

FIGURE 13. The multiharmonic finite element approximations u_{Nh} to the control u with $N = 5$ for $\lambda = 1, 10^{-2}, 10^{-4}, 10^{-6}$ as functions of time in $[0, 1]$ at the spatial coordinates $(0.5, 0.5)$ for $\omega = 1$ and with jumping material coefficients (Example 5).

the time-periodic parabolic optimal control problem, where all functions are approximated by truncated Fourier series and the Fourier coefficients by the finite element method. The optimality system decouples into smaller systems corresponding to every single mode. Furthermore, we have provided a rigorous discretization error

n_{iter}	λ								
grid	10^{-8}	10^{-6}	10^{-4}	10^{-2}	1	10^2	10^4	10^6	10^8
64×64	12	9	12	21	23	20	18	16	14
128×128	12	10	18	21	26	22	18	16	16
256×256	12	15	22	23	28	20	18	16	16
512×512	13	22	24	22	28	22	20	18	18

TABLE 9. Number of MINRES iterations n_{iter} for different values of λ on grids of different mesh size (Example 5)

time(in s)	λ								
grid	10^{-8}	10^{-6}	10^{-4}	10^{-2}	1	10^2	10^4	10^6	10^8
64×64	0.12	0.10	0.12	0.21	0.24	0.20	0.18	0.17	0.13
128×128	0.61	0.50	0.88	1.01	1.27	1.08	0.88	0.79	0.79
256×256	2.67	3.29	4.57	5.01	6.22	4.46	4.05	3.60	3.60
512×512	12.26	20.04	21.72	20.83	26.47	21.00	19.09	17.25	17.24

TABLE 10. The computational times in seconds for different values of λ on grids of different mesh size (Example 5)

analysis including the estimates for the truncation error in N and the spatial error in terms of h.

We have solved the optimality system by the preconditioned MINRES method, where we have used the AMLI preconditioner from [24] for the efficient implementation of our MINRES precondioner. The MINRES preconditioner is robust with respect to all parameters including also a possibly vanishing parameter σ which corresponds to the conductivity in practical applications, see also [20]. The parallel implementation of the computation of the Fourier coefficients for different modes is straithforward.

Finally, we present also new numerical results for this class of optimal control problems as well as compare them to the results in [1]. In our numerical examples, we could compute the Fourier coefficients of the desired state exactly. Hence, the efficient numerical computation of the Fourier coefficients together with an error analysis is a matter of future work.

Altogether, the theoretical as well as the numerical results show that the multiharmonic finite element method is a robust and efficient technique for solving time-periodic parabolic optimal control problems without inequality contraints for the control and the state. However, inequality contraints imposed on the Fourier coefficients of the state or the control can easily be included into the multiharmonic finite element approach, although one loses the robustness with respect to the cost or regularization parameter when solving the optimality system by the preconditioned MINRES method, see [19]. The inclusion of inequality constraints imposed on the state or the control itself is much harder to handle. One can include them as penalty term in the cost functional. This approach yields a nonlinear optimality system. Nonlinearities of this kind, but also nonlinearities arising from nonlinear PDEs as in the case of coefficients which depend on the solution (e.g. $\nu = \nu(\nabla y)$ or $\nu = \nu(y)$) lead to coupled nonlinear optimality systems. The Newton linearization results in linear systems where all modes are coupled. However, the preconditioners studied here can be very useful for the efficient solution of the linear systems arising at each step of the Newton method, see [7] for the solution of time-periodic eddy current problems.

Acknowledgment

The research has been supported by the Doctoral Program "Computational Mathematics: Numerical Analysis and Symbolic Computation". The authors gratefully acknowledge the financial support by the Austrian Science Fund (FWF) under the grant W1214, project DK4, the Johannes Kepler University of Linz and the Federal State of Upper Austria.

References

[1] D. Abbeloos, M. Diehl, M. Hinze, and S. Vandewalle. Nested multigrid methods for time-periodic, parabolic optimal control problems. *Comput. Vis. Sci.*, 14(1):27–38, 2011.

[2] R. Adams and J. Fournier. *Sobolev spaces. Second Edition.* Academic Press, 2008. Volume 140 in the Pure and Applied Mathematics series, Elsevier.

[3] I. Babuška. Error-bounds for finite element method. *Numer. Math.*, 16:322–333, 1971.

[4] I. Babuška and A. Aziz. Survey lectures on the mathematical foundation of the finite element method. *The Mathematical Foundation of the Finite Element Method with Applications to Partial Differential Equations (A.K. Aziz, ed.), Academic Press, New York – London*, pages 3–345, 1972.

[5] F. Bachinger, M. Kaltenbacher, and S. Reitzinger. An efficient solution strategy for the hbfe method. *Proceedings of the IGTE '02 Symposium Graz, Austria*, pages 385–389, 2005.

[6] F. Bachinger, U. Langer, and J. Schöberl. Numerical analysis of nonlinear multiharmonic eddy current problems. *Numer. Math.*, 100:593–616, 2005.

[7] F. Bachinger, U. Langer, and J. Schöberl. Efficient solvers for nonlinear time-periodic eddy current problems. *Comput. Vis. Sci.*, 9(4):197–207, 2006.

[8] J. Bergh and J. Löfström. *Interpolation spaces: An introduction.* Springer-Verlag, Berlin-Heidelberg-New York, 1976.

[9] A. Borzi and V. Schulz. *Computational optimization of systems governed by partial differential equations*, volume 8 of *SIAM book series on Computational Science and Engineering.* SIAM, Philadelphia, 2012.

[10] P. Ciarlet. *The finite element method for elliptic problems.* North-Holland Publishing Company, Amsterdam-New York-Oxford, 1978. Republished by SIAM in April 2002.

[11] D. Copeland, M. Kolmbauer, and U. Langer. Domain decomposition solvers for frequency-domain finite element equation. *Domain Decomposition Methods in Science and Engineering XIX of Lecture Notes in Computational Science and Engineering, Springer*, 78:301–308, 2011.

[12] D. Copeland and U. Langer. Domain decomposition solvers for nonlinear multiharmonic finite element equations. *Numer. Math.*, 18(3):157–175, 2010.

[13] H. de Gersem, H. Sande, and K. Hameyer. Strong coupled multiharmonic finite element simulation package. *COMPEL*, 20:535–546, 2001.

[14] W. Gong, M. Hinze, and Z. Zhou. Space-time finite element approximation of parabolic optimal control problems. *J. Numer. Math.*, 20(2):111–145, 2012.

[15] A. Greenbaum. *Iterative Methods for Solving Linear Systems.* Society for Industrial and Applied Mathematics (SIAM), Philadelphia, PA, 1997.

[16] J. Gyselinck, P. Dular, C. Geuzaine, and W. Legros. Harmonic-balance finite-element modeling of electromagnetic devices: a novel approach. *IEEE Transactions on Magnetics*, 38(2):521–524, 2002.

[17] W. Hackbusch. Fast numerical solution of time-periodic parabolic problems by a multigrid method. *SIAM J. Sci. Comput.*, 2(2):198–206, 1981.

[18] R. Hiptmair. Operator preconditioning. *Comput. Math. Appl.*, 52:699–706, 2006.

[19] M. Kollmann and M. Kolmbauer. A preconditioned minres solver for time-periodic parabolic optimal control problems. *Numer. Linear Algebra Appl.*, 2012.

[20] M. Kollmann, M. Kolmbauer, U. Langer, M. Wolfmayr, and W. Zulehner. A finite element solver for a multiharmonic parabolic optimal control problem. *Comput. Math. Appl.*, 65(3):469–486, 2013.

[21] M. Kolmbauer. Efficient solvers for multiharmonic eddy current optimal control problems with various constraints and their analysis. *IMA J. Numer. Anal.*, 2012. (to appear).

[22] M. Kolmbauer. A robust FEM-BEM MinRes solver for distributed multiharmonic eddy current optimal control problems in unbounded domains. *Electron. Trans. Numer. Anal.*, 39:231–252, 2012.

[23] M. Kolmbauer and U. Langer. A robust preconditioned-minres-solver for distributed time-periodic eddy current optimal control problems. *SIAM J. Sci. Comput.*, 34(6):B785–B809, 2012.

[24] J. Kraus. Additive schur complement approximation and application to multilevel preconditioning. *SIAM J. Sci. Comput.*, 34(6):A2872–A2895, 2012.

[25] J. Kraus and S. Margenov. *Robust Algebraic Multilevel Methods and Algorithms*, volume 5 of *Radon Series on Computational and Applied Mathematics*. de Gruyter, Berlin, 2009.
[26] W. Krendl, V. Simoncini, and W. Zulehner. Stability estimates and structural spectral properties of saddle point problems. *Numer. Math.*, 2012. (published online).
[27] O. A. Ladyzhenskaya, V. A. Solonnikov, and N. N. Ural'ceva. *Linear and Quasilinear Equations of Parabolic Type*. American Math. Society, Providence, R.I., 1968.
[28] G. M. Lieberman. Time-periodic solutions of linear parabolic differential equations. *Comm. Partial Differential Equations*, 24:631–663, 1999.
[29] K.-A. Mardal and R. Winther. Preconditioning discretizations of systems of partial differential equations. *Numer. Linear Algebra Appl.*, 18(1):1–40, 2011.
[30] C. Paige and M. Saunders. Solution of sparse indefinite systems of linear equations. *SIAM J. Numer. Anal.*, 12(4):617–629, 1975.
[31] G. Paoli, O. Bíro, and G. Buchgraber. Complex representation in nonlinear time harmonic eddy current problems. *IEEE Transactions on Magnetics*, 34(5):2626–2628, 1998.
[32] J. W. Pearson and A. J. Wathen. A new approximation of the schur complement in preconditioners for pde-constrained optimization. *Numer. Linear Algebra Appl.*, 19(5):816–829, 2012.
[33] C. Pechstein. *Finite and Boundary Element Tearing and Interconnecting Solvers for Multiscale Problems*. Springer-Verlag, Berlin, Heidelberg, New York, 2012.
[34] J. Schöberl and W. Zulehner. Symmetric indefinite preconditioners for saddle point problems with applications to pde-constrained optimization problems. *SIAM J. Matrix Anal. Appl.*, 29(3):752–773, 2007.
[35] A. Toselli and O. Widlund. *Domain Decoposition Methods - Algorithms and Theory*, volume 34 of *Springer Series in Computational Mathematics*. Springer, Berlin, Heidelberg, 2004.
[36] F. Tröltzsch. *Optimal Control of Partial Differential Equations. Theory, Methods and Applications*. Graduate Studies in Mathematics 112, American Mathematical Society (AMS), Providence, RI, 2010.
[37] F. Tröltzsch and I. Yousept. PDE-constrained optimization of time-dependent 3D electromagnetic induction heating by alternating voltages. *ESAIM: M2AN*, 46:709–729, 2012.
[38] S. Vandewalle and R. Piessens. Efficient parallel algorithms for solving initial-boundary value and time-periodic parabolic partial differential equations. *SIAM J. Sci. Stat. Comput.*, 13(6):1330–1346, 1992.
[39] S. Vandewalle and R. Piessens. On dynamic iteration methods for solving time-periodic differential equations. *SIAM J. Numer. Anal.*, 30(1):286–303, 1993.
[40] P. Vassilevski. *Multilevel Block Factorization Preconditioners: Matrix-based Analysis and Algorithms for Solving Finite Element Equations*. Springer, New York, 2008.
[41] S. Yamada and K. Bessho. Harmonic field calculation by the combination of finite element analysis and harmonic balance method. *IEEE Transactions on Magnetics*, 24(6):2588–2590, 1988.
[42] E. Zeidler. *Nonlinear Functional Analysis and its Applications II/A: Linear Monotone Operators*. Springer, New York, 1990.
[43] E. Zeidler. *Nonlinear Functional Analysis and its Applications II/B: Nonlinear Monotone Operators*. Springer, New York, 1990.
[44] W. Zulehner. Nonstandard norms and robust estimates for saddle point problems. *SIAM J. Matrix Anal. Appl.*, 32(2):536–560, 2011.

(U. Langer, M. Wolfmayr) Institute of Computational Mathematics, Johannes Kepler University Linz, Altenberger Strasse 69, A-4040 Linz, Austria/Europe
E-mail address: ulanger@numa.uni-linz.ac.at
E-mail address: monika.wolfmayr@numa.uni-linz.ac.at

Latest Reports in this series

2009 - 2011

[..]

2012

2012-01	Markus Kollmann and Walter Zulehner *A Robust Preconditioner for Distributed Optimal Control for Stokes Flow with Control Constraints*	January 2012
2012-02	Michael Kolmbauer and Ulrich Langer *A Robust Preconditioned MinRes-Solver for Time-Periodic Eddy Current Problems*	January 2012
2012-03	Wolfgang Krendl, Valeria Simoncini and Walter Zulehner *Stability Estimates and Structural Spectral Properties of Saddle Point Problems*	February 2012
2012-04	Helmut Gfrerer *On Directional Metric Regularity, Subregularity and Optimality Conditions for Nonsmooth Mathematical Programs*	February 2012
2012-05	Veronika Pillwein and Stefan Takacs *A Multigrid Fourier Analysis of a Multigrid Method using Symbolic Computation*	April 2012
2012-06	Stefan Takacs and Walter Zulehner *Convergence Analysis of All-at-once Multigrid Methods for Elliptic Control Problems Under Partial Elliptic Regularity*	June 2012
2012-07	Helmut Gfrerer *On Directional Metric Subregularity and Second-Order Optimality Conditions for a Class of Nonsmooth Mathematical Programs*	August 2012
2012-08	Michael Kolmbauer and Ulrich Langer *Efficient Solvers for Some Classes of Time-Periodic Eddy Current Optimal Control Problems*	November 2012
2012-09	Clemens Hofreither, Ulrich Langer and Clemens Pechstein *FETI Solvers for Non-Standard Finite Element Equations Based on Boundary Integral Operators*	November 2012
2012-10	Helmut Gfrerer *On Metric Pseudo-(sub)Regularity of Multifunctions and Optimality Conditions for Degenerated Mathematical Programs*	December 2012
2012-11	Clemens Pechstein and Clemens Hofreither *A Rigorous Error Analysis of Coupled FEM-BEM Problems with Arbitrary Many Subdomains*	December 2012
2012-12	Markus Eslitzbichler, Clemens Pechstein and Ronny Ramlau *An H^1-Kaczmarz Reconstructor for Atmospheric Tomography*	December 2012
2012-13	Clemens Pechstein *On Iterative Substructuring Methods for Multiscale Problems*	December 2012

2013

2013-01	Ulrich Langer and Monika Wolfmayr *Multiharmonic Finite Element Analysis of a Time-Periodic Parabolic Optimal Control Problem*	January 2013

From 1998 to 2008 reports were published by SFB013. Please see
`http://www.sfb013.uni-linz.ac.at/index.php?id=reports`
From 2004 on reports were also published by RICAM. Please see
`http://www.ricam.oeaw.ac.at/publications/list/`
For a complete list of NuMa reports see
`http://www.numa.uni-linz.ac.at/Publications/List/`